# DNA Detection Using Organic Thin Film Transistors: Physical Origins of Electrical Transduction Behavior and Optimization of Sensitivity

*Lakshmi Jagannathan*
*Vivek Subramanian*

Electrical Engineering and Computer Sciences
University of California at Berkeley

Technical Report No. UCB/EECS-2009-11
http://www.eecs.berkeley.edu/Pubs/TechRpts/2009/EECS-2009-11.html

January 22, 2009

# DNA Detection Using Organic Thin Film Transistors: Physical Origins of Electrical Transduction Behavior And Optimization of Sensitivity

by Lakshmi Jagannathan

Submitted to the Department of Electrical Engineering and Computer Sciences, University of California at Berkeley, in partial satisfaction of the requirements for the degree of **Master of Science, Plan II**.

Approval for the Report and Comprehensive Examination:

**Committee:**

Professor Vivek Subramanian
Research Advisor

Date:

* * * * * * *

Professor Ali Javey
Second Reader

Date:

# Acknowledgements

I am indebted to many people for directly and indirectly helping me with this thesis. I want to thank my advisor, Vivek Subramanian, for his advice and support throughout. He has been a great role model, and I have learned a lot working with him for the past few years. I would also like to thank our entire EECS Organic Electronics group at Berkeley, for their advice, encouragement, knowledge transfer, immediate willingness to help, and in general, just making me love to come to the office everyday ☺. I am grateful to Dr. Qintao Zhang, a graduate from our group, for the knowledge transfer of the biosensor system, and his willingness to help to this day. I would also like to thank Dr. Kanan Puntambekar, a postdoc graduate from our group, for helping me better understand and explain different aspects of my project. I want to thank Daniel Forchheimer for his help with the DNA microfluidics experiment, and his contribution of valuable ideas to my project. I would like to express thanks to Professor Ali Javey for being a second reader for my thesis, and for his encouragement during my first years in graduate school at Berkeley. I want to also acknowledge Dr. Steve Ruzin and the staff at the College of Natural Resources, for their training and help with the fluorescent microscopy system. I want to thank Ruth Gjerde and Pat Hernan at Berkeley for their constant encouragement; they always believed in me more than I did! I would like to thank Semiconductor Research Corporation (SRC) and Intel for sponsoring and funding me for graduate school. I am grateful to Karen, Soundarya, Bharath, Kristen, Sridevi, Dhevi, and Shalini, for their constant support and encouragement, and in particular for proofreading this document. I want to also thank my entire youth group for their encouragement and help with everything. I would like to thank all of my friends for being there for me when I needed them. Finally, I want to express my heartfelt gratitude to my spiritual guru and guide, Sri Sathya Sai Baba, my entire family in Dallas, and my family in San Jose for their love and incredible support, without which this truly would have not been possible!

# Table of Contents

# List of Figures

## List of Tables

# I. Introduction

## A. Abstract

Advancements in research and technology are happening now more than ever in the biotechnology industry. Better detection and treatment methods are constantly being sought by researchers. Collaboration among different fields of science and technology has brought us one step closer towards achieving this goal. The vision of achieving a personalized system of disease detection and treatment has triggered the ultimate purpose of my project: to be able to detect genetic diseases using electrical means of sensing and detection. Previous work has shown the potential of organic (pentacene) thin film transistors (OTFT) for DNA detection by showing different electrical performance shifts in response to single and double stranded DNA[5]. The goal of this thesis is to present two aspects of using OTFTs for genetic disease detection, namely the physical origins of the observed electrical shifts, and the characterization of the pentacene surface to allow optimization of the same for DNA immobilization and sensor sensitivity.

## B. Motivation

Using OTFTs for DNA (Deoxyribonucleic acid) microarray technology paves the path for an ideal DNA detection system. DNA detection is important to detect mutations that cause genetic diseases. A genetic disorder is a disease that is caused by an abnormality in an individual's DNA. Abnormalities can range from a small mutation in a single gene to the addition or subtraction of an entire chromosome or set of chromosomes.

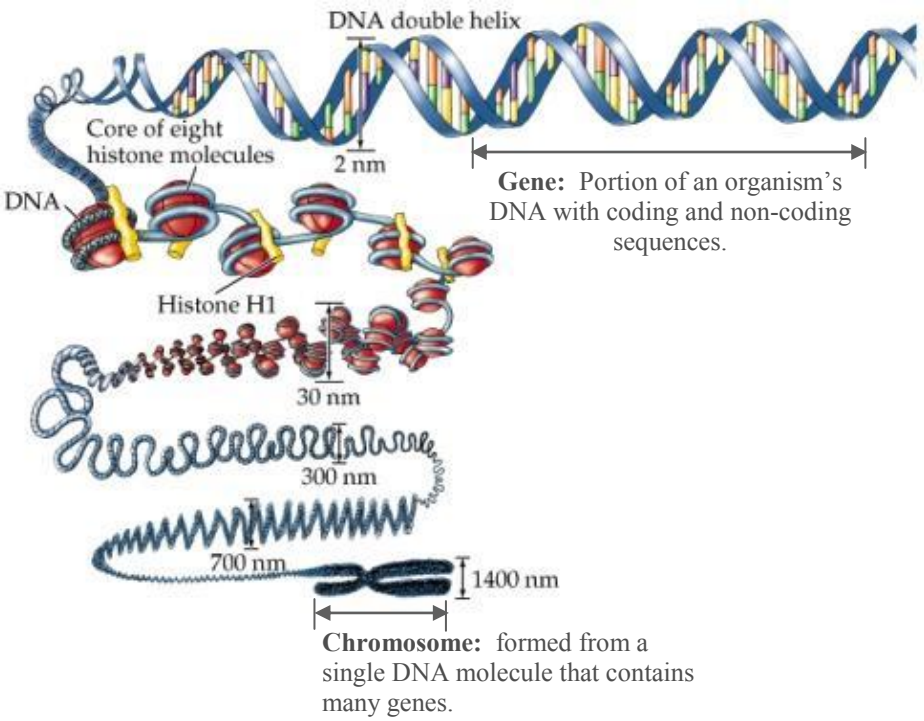


**Figure 1.** DNA is a building block for everything within a human being [1].

An ideal detection system would consist of an ultra low-cost, disposable DNA detection chip, which can be analyzed with a handheld device (e.g. PDA), using a quick and easy testing protocol. Moreover, the results/feedback from the chip would be available within a few hours.

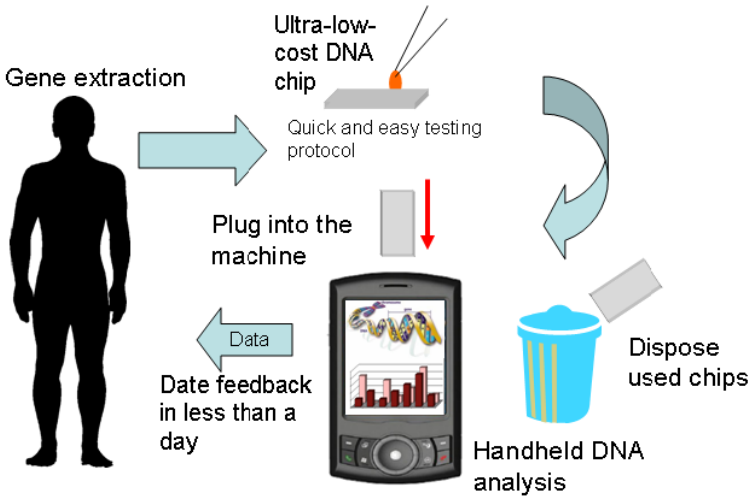


**Figure 2.** An Ideal DNA Detection System.
*(Image: Courtesy of Dr.Qintao Zhang, Graduate from EECS Organics Electronics Group, UC Berkeley)*

Use of organic transistors facilitates the possibility of an ultra low-cost, disposable DNA chip through printed electronics. Ultra-low cost printed electronics have gained a great deal of interest over the past few years because of their promise to greatly reduce the cost of many electronic applications. They seek to reduce the manufacturing cost of electronics with less expensive, all-additive printing methods that conventional silicon manufacturing cannot replicate. There are several applications for low-cost printed electronics including radio frequency identification (RFID) tags, electronic sensors, displays, smart cards, packaging, and printed circuit boards (PCB). Based on performance requirements for the above applications, suitable electronic materials for printing are typically examined, characterized, and implemented. For example, soluble gold nanoparticle ink for metallization, printable organic dielectrics including polyimide and PVP, and a high performance organic semiconductor such as a pentacene precursor semiconductor ink have all been used to make a fully printed organic thin film transistor [2]. All of these materials have plastic substrate compatible activation temperatures (<200°C).

Printed electronics using organic semiconductors have many advantages over typical silicon processes. Although silicon processing uses many of the ideas in printing to achieve low costs and rapid manufacturing, certain limitations make it difficult to reduce costs further. Some of the high costs associated with silicon processing include energy because of the high thermal budget and requirement of ultra-clean processes, and the capital and process cost expenditures associated with pattern transfer or photolithography due to the extra time and material (>90% material wasted overall) needed by the lithography processing steps [2]. The processing steps for printed electronics have a low thermal budget, allowing for a variety of low-cost and flexible substrates, and additive processing, through which material is only deposited where needed, reducing the overall consumption of materials. Figure 3 depicts the process flow for printed OTFTs.

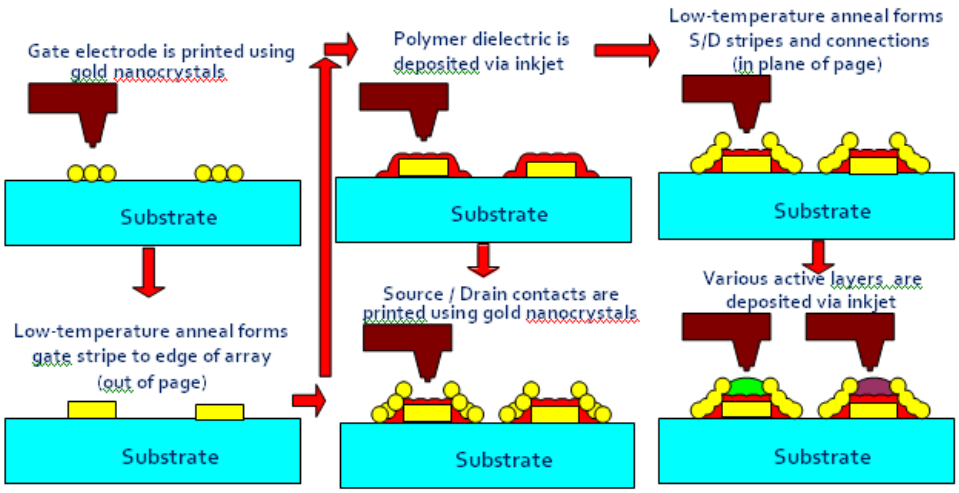


**Figure 3.** Process flow for formation of printed FETs.
*(Image: Courtesy of Dr.Vivek Subramanian, UC Berkeley)*

Printed OTFTs are particularly suitable for sensor applications because of the ability to print multiple active layers on the same substrate and the bottom gated structure. The ability to print multiple layers on the same substrate is very valuable for biosensor applications because it gives the DNA microarray technology (explained in the following section) another dimension. The bottom gated structure allows for the channel layer to be exposed. This allows for easy and non-destructive inclusion of analytes, bio-molecules/proteins, etc., as the final 'layer.' Moreover, the open channel layer allows for easy electrical measurements before and after inclusion of the objects that are to be sensed. DNA sensitivity is measured using the saturation current before and after the immobilization of DNA. Having this layer open is critical for this step in the experiment to take place.

In this work, evaporated pentacene transistors were used instead. As we will discuss later in the thesis, the morphology of the pentacene surface is critical to the immobilization of the DNA and the sensitivity of the sensor. By evaporating pentacene instead of printing it, we are able to control this surface structure very precisely. For the purposes of the work covered in this thesis, the control of this surface was very important for optimization. Therefore, evaporated pentacene

transistors were used. Translating from evaporated to printed transistors, in terms of the fabrication processes and output characteristics, has previously been mastered by our group and will be implemented in the future work of this project.

## C. Pentacene Organic Thin Film Transistors for Biosensing

The pentacene TFT bottom gated structure used throughout this project is shown in Figure 4 below.

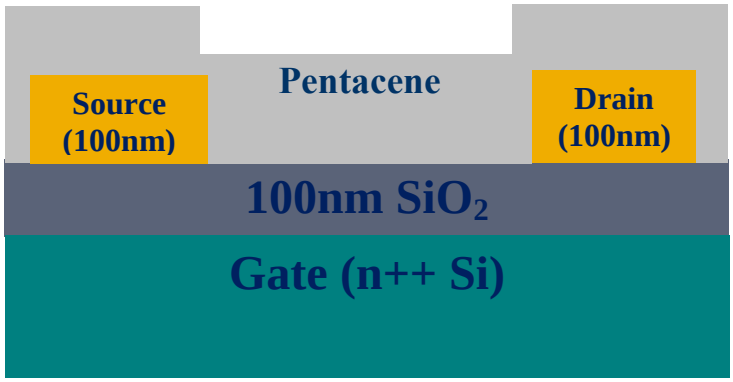


**Figure 4.** Pentacene TFT Structure.

The thickness of the pentacene can be varied as necessary, but for our purposes, it ranges from 10-30nm. The steps for fabricating the transistor and including DNA on the pentacene surface will be discussed further in chapter IV of the thesis.

Pentacene TFTs are potentially useful for biosensors because of the advantages they provide over current state of the art fluorescent detection technology. The current DNA microarray/chip technology involves a meticulous process. For example, to determine whether an individual possesses a mutation for BRCA1 or BRCA2, genes whose mutations are known to cause as many as 60% of all cases of hereditary breast and ovarian cancers [3], a scientist first obtains a sample of DNA from the patient's blood as well as a control sample, one that does not contain a mutation in either gene. The researcher then denatures the DNA in the samples, a process that separates

the two complementary strands of DNA into single-stranded molecules. The long strands of DNA are then cut into smaller, more manageable fragments. Each fragment is then labeled by attaching a fluorescent dye. The individual's DNA is labeled with green dye and the control (normal) DNA is labeled with red dye. Both sets of labeled DNA are then inserted into the chip and allowed to hybridize (bind) to the synthetic BRCA1 or BRCA2 DNA on the chip.

If the individual does not have a mutation for the gene, both the red and green samples will bind to the sequences on the chip. If the individual does possess a mutation, the individual's DNA will not bind properly in the region where the mutation is located. The scientist can then examine this area more closely to confirm that a mutation is present [3].

With our pentacene TFT sensor, we propose to do the same mutation detection electrically. Instead of using fluorescent laser technology to correlate the extracted fluorescent signals with mutations, we will detect the mutations by analyzing conductance and threshold voltage shifts. Our technology has several advantages compared to the current optical detection technology:

1) *Higher Sensitivity:* As many previous researchers have already shown, electrical detection is known to be more sensitive than optical detection [4]. If the detector is more sensitive, needless to say, the diseases can be detected earlier (important for early cancer detection, for example) and much more accurately.

2) *Label free method:* The DNA used with our proposed technology does not need to be tagged with fluorescent molecules. This means that the expensive fluorescent laser detection system can also be eliminated. The whole process becomes simpler and cheaper.

3) *Disposable/Portable/Ultra-low cost:* Adding to the previous point, the elimination of the fluorescent laser detection system makes it cheaper and easily accessible. Also, since

OTFTs can potentially be printed on plastic substrates, the disposability and low-cost factors are further made easier. More importantly, it is impossible to make a disposable DNA detection chip unless it is done with an electrical or a label-free method.

4) *Faster Process:* The method of hybridization, which takes 12-24 hours, poses a bottleneck for the current DNA microarray technology process. Amongst other steps that could potentially save time in our proposed technology, the possibility of pulse-enhanced hybridization [5], which could potentially reduce the hybridization time to milliseconds, makes our proposed electrical detection process much faster.

Having thus motivated and introduced the topic, the next few sections will discuss the sensor system further. Section II describes the immobilization and doping mechanisms of DNA on pentacene. Section III discusses the methods that have been used and will be used to correlate the amount of DNA on the surface with the electrical shift observed. Finally, Section IV will present the effect of pentacene film formation on DNA detection behavior, and optimization of the pentacene surface in terms of morphology and topology for highest DNA immobilization, and more importantly, highest sensitivity for DNA detection.

# II. DNA Immobilization and Doping

## A. DNA Immobilization on Pentacene Film

Previously, it has been shown that pentacene can be used to detect DNA [5]. Through physical absorptive immobilization, DNA immobilizes on pentacene film. The pentacene film is hydrophobic, and DNA is diluted in saline-sodium citrate (SSC) buffer solution. The 20x solution of buffer consists of 3M sodium chloride and 300 mM trisodium citrate. The buffer solution is further diluted in water, as it is usually done in practice, to give a 2x concentration solution. The buffer can be considered salt water for analytical purposes.

The hydrophobic interaction immobilization (interactions between ssDNA molecules and crevices on hydrophobic substrate surface) was a very common method in the early stage of DNA microarray development and has been studied very well [6]. Using this method, we can explain the pentacene film interaction with DNA. When the DNA in buffer solution is pipetted onto the pentacene surface, the DNA segregates to hydrophobic 'holes' on the surface. During this process, the salt water, in which the DNA is diluted, gets pushed out, 'physically' immobilizing the DNA in these crevices.

Initial hypotheses led us to believe that roughness and grain boundaries in particular immobilize more DNA, and would give the highest sensitivity. Recent experiments, which will be presented in later sections of the thesis, have shown that in addition to the morphological features, the overall sensitivity is more strongly dependent on how much DNA is able to diffuse to the part of the pentacene film which contains the channel. The channel is contained within the first few monolayers of pentacene film.

## B. DNA and Pentacene Interaction

The sensing of DNA is possible because of DNA interaction with pentacene. The DNA and pentacene chemical structures are shown in Figure 5a and 5b below:

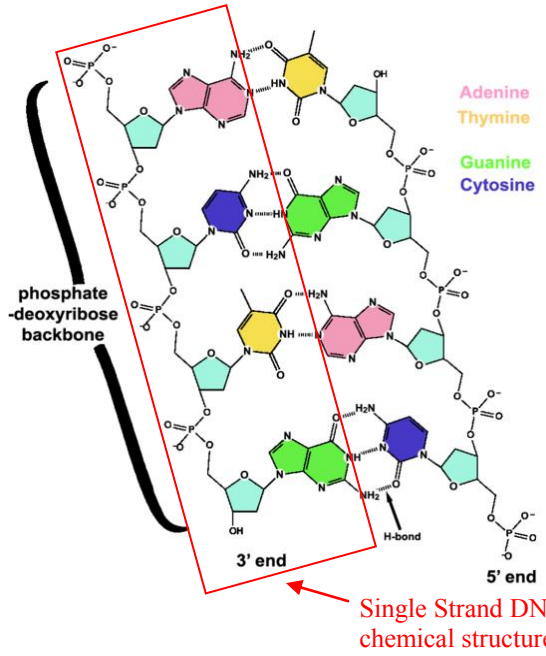


**Figure 5a.** Double stranded DNA chemical structure [7].

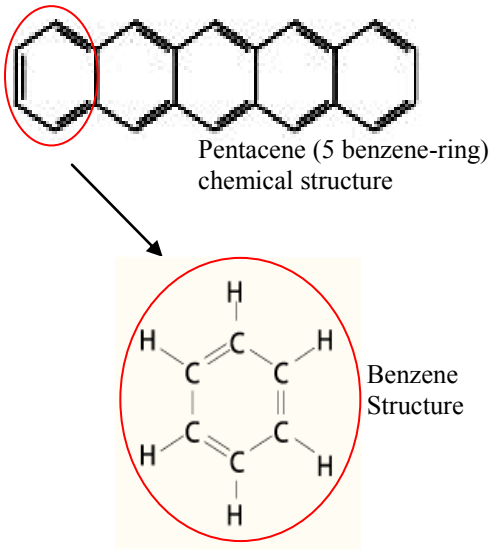


**Figure 5b.** Pentacene (5-benzene ring) chemical structure [8].

Pentacene TFTs are p-type accumulation devices (negative gate voltage and negative current). After DNA immobilization on surface, the hole current of the TFT increases. Consequently, the threshold voltage ($V_t$) becomes more positive (i.e. shifts to the right). The result from one of the experiments, shown in Figure 6 below, delineates the sensor characteristics observed after DNA interaction with pentacene.

$I_{on}$ Ratio is defined as:

$$\mathbf{I_{on}\ Ratio} = \frac{I_d\,(DrainCurrent)\,AfterDNA\,\mathrm{Im}mobilization}{I_d\,BeforeDNA\,\mathrm{Im}mobilization}$$

The bigger the $I_{on}$ Ratio, the higher the sensitivity of the sensor. The DNA used in the experiment below and all of the experiments/results that will be presented in the thesis, is a 125-base pair designed single strand DNA sequence, synthesized by Biosynthesis, Inc.

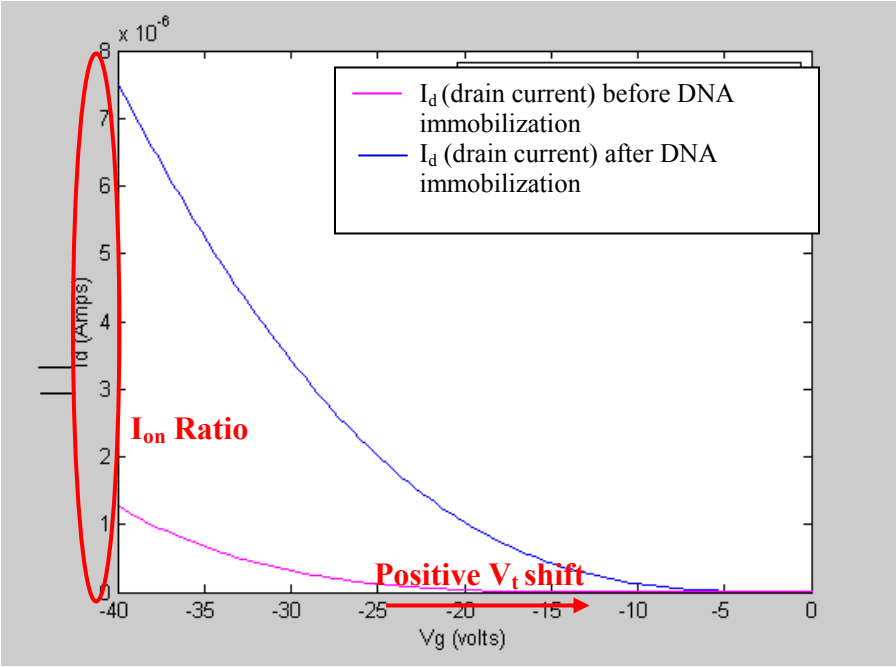


**Figure 6.** Current-Voltage characteristics from an experiment show a positive $V_t$ shift and a higher hole current after DNA immobilization.

Two possible explanations of the interaction of DNA and pentacene will be discussed below. One is the direct doping of DNA on pentacene. The net-effect of the DNA on the pentacene surface is electron withdrawing, therefore increasing the hole current of the transistor. Although DNA is known to be negatively charged because of the phosphate groups on its backbone, the possible interaction of the two chemical structures shown in Figure 5 might be causing the shift in hole current. More specifically, areas of interaction include the aromatic structures in base pairs (such as adenine) of the DNA, and the inherent aromaticity of the 5 benzene-ring pentacene structure. The result of this electron withdrawing interaction is supported and explained below using the Kelvin Probe Microscopy technique.

Another explanation uses the trap filling caused by the electrical interactions with DNA to improve the overall performance of the transistor, resulting in the shift seen in Figure 6. Using SCLC (Space Charge Limited Current) measurement technique, Zhang et al are able to support this hypothesis. A short summary of Dr. Zhang's work on these explanations is discussed below.

Further details on the doping mechanisms of DNA can be found in his thesis, *OTFT Based DNA Detection System.*

Dr. Zhang performed Atomic Force Microscopy (AFM) measurements to verify the DNA doping of pentacene. Figure **7** below shows an AFM image of a DNA molecule along with potential measurements done through Kelvin probe microscopy [5].

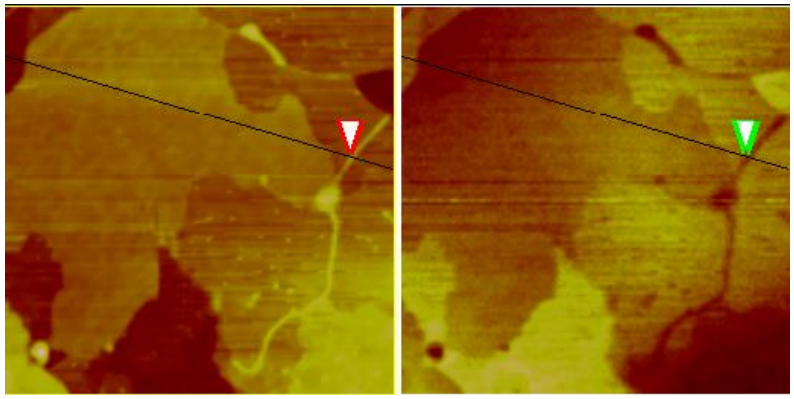

**a)**


**b)**

**Figure 7**. Surface potential measurement of DNA molecules on a pentacene film. a) An Atomic Force Microscopy (AFM) image, where the single bright thread is an immobilized DNA molecule. b) A surface potential image matching the same area of the AFM image on the top. It is clear that the DNA molecule has negative potential, which is possibly caused by electron-withdrawing from the bottom pentacene film [5].

Kelvin Probe Force Microscopy (KPFM) is a scanned probe method where the potential offset between a probe tip and a surface can be measured using the same principle as a macroscopic Kelvin probe. The cantilever in the AFM is a reference electrode that forms a

capacitor with the surface, over which it is scanned laterally at a constant separation. With KPFM the workfunction of surfaces can be observed at atomic or molecular scales. The work function relates to many surface phenomena, including catalytic activity, reconstruction of surfaces, doping and band-bending of semiconductors, charge trapping in dielectrics and corrosion [12]. Unlike workfunction mismatch induced surface potential seen in solid thin film study though, the surface potential of macro bio-molecules is caused by dipoles. DNA hybridization or antigen-antibody reactions have been proved to increase the amplitude of potential differences [11]. The bright thread seen in Figure 7a (shown by the green and red arrows on the image) represents DNA. The KPFM results in Figure 7b show that at the location of the DNA, the potential becomes negative indicating that DNA, as a result of the immobilization and interaction with the pentacene surface, has become more negatively charged. Given these results of the KPFM measurements, Dr. Zhang is able to conclude that the DNA molecule has negative potential, possibly caused by electron-withdrawing from the bottom pentacene film [5].

A space charge limited current (SCLC) measurement explains the doping mechanism as well. SCLC is a result of the space charge region that forms within a conductive semiconductor material where the charge carriers have diffused away, or have been forced away by an electric field. Space charge regions have been shown to exist in pentacene films with gold electrodes in previous studies [29]. The space charge region is characterized by generation-recombination centers, steep impurity gradients, and rapidly changing populations of holes and electrons. This space charge region limits the current carried by the majority carriers because of the presence traps within this region. The electrical impact of DNA, with its negative charge, is to fill these traps, facilitating the flow of hole current.

An SCLC setup measures two-terminal devices. A voltage from 0 to 100V is swept between the source/drain with a floating gate electrode, and the current flowing into the drain is measured.

A typical SCLC curve is plotted on a log-log scale and has more than two different slopes. The slope=1 part of the curve is called ohmic regime and the slope≥ 2 part is the trap-filling regime. As the electrical field is increased to a certain level, the concentration of the injected carriers from the electrode overwhelms the intrinsic carrier concentration, thus starting to fill traps in the films. At a slope very close to 2, all traps been filled. This trap-free regime, slope equal 2, is also called SCLC regime [5]. The SCLC curve, measured by Dr. Zhang, is shown in Figure 8 below.

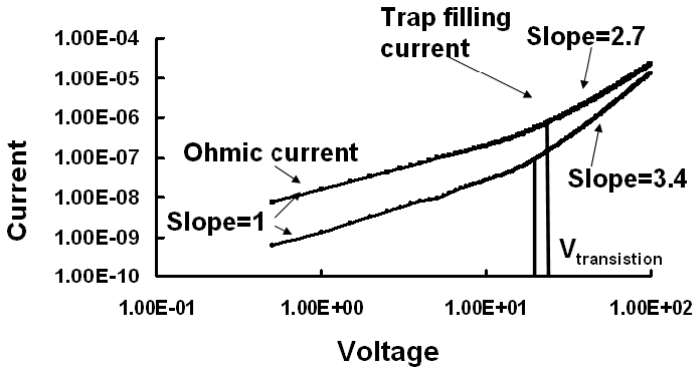


**Figure 8.** Representative SCLC curves of original pentacene-based transistors and DNA immobilized transistors [5].

SCLC measurements before and after DNA immobilization shown above illustrate the doping mechanism of DNA molecules on the pentacene film. In the ohmic regime, the magnitude of current increased, relating to the free carrier concentration increase or mobility increase, because of immobilized DNA segments. In the trap-filling regime, the decrease in slope from 3.4 as measured in the original pentacene transistor to 2.7 in the DNA immobilized pentacene transistors indicates that deep traps have been filled by DNA molecules. Figure 8 shows that the trap-filling action in hole-rich pentacene film has actually increased the hole concentration. This is because trapped electrons in the pentacene film have been released by DNA segments, thereby facilitating the flow of hole current [5, 6].

# III. Investigation of Physical Origins of Electrical Transduction Behavior

An important step in making a viable DNA sensor is to show that what is being detected is just the DNA, and to eliminate any other noise that might affect the sensitivity. One way to do this is to correlate the amount of DNA on the surface with the electrical shift that is seen after DNA immobilization. A few methods were used to obtain this data, namely atomic force microscopy (AFM), fluorescent microscopy, and time-of-flight secondary ion mass spectroscopy (TOF-SIMS). Useful results and insight were derived from the latter two techniques and are discussed in this section.

## A. Fluorescent Microscopy

Fluorescent microscopy is a light microscope used to study properties of organic or inorganic substances using the phenomena of fluorescence and phosphorescence instead of, or in addition to, reflection and absorption. A component of interest in the specimen is specifically labeled with a fluorescent molecule called a fluorophore (such as green fluorescent protein (GFP), fluorescein).

The ssDNA used in this experiment was tagged with carboxyfluorescein molecule on the 5'end of the DNA strand. Carboxyfluorescein is a fluorescent dye with an excitation and emission of 492/517 nm, respectively. In other words, the DNA with the fluorescent molecule is illuminated with light of wavelength of 492nm which is absorbed by the fluorophores. It then emits a light of wavelength of 517nm, which is in turn passed by an emission filter specific to the emitted wavelength. The illumination light is separated from the much weaker emitted fluorescence through the use of the emission filter. Typical components of a fluorescence microscope are the light source (xenon arc lamp or mercury-vapor lamp), the excitation filter, the

dichroic mirror (or dichromatic beamsplitter), and the emission filter [14]. Figure 9 below delineates the fluorescent microscopy system.

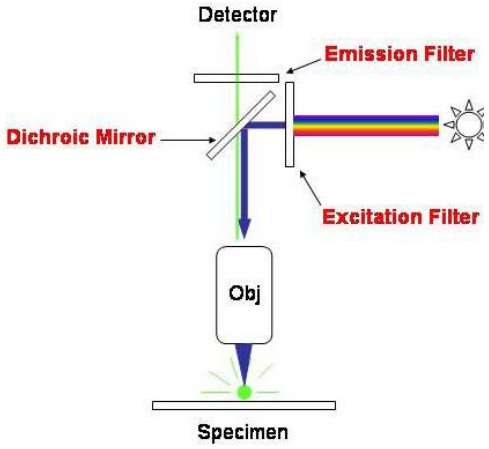


**Figure 9.** Fluorescent Microscope System [13].

A Zeiss AxioImager M1 fluorescence microscope system from the College of Natural Resources, Berkeley, was used in this experiment. The microscope contains the Photometrics Quantix digital CCD camera that allows visualization of fluorescence with high spatial resolution (1200X1300 pixels) and high bit depth (12-bit gray scale). A second camera, QImaging 5MPix MicroPublisher, captures color images. The set-up is shown in Figure 10 below.

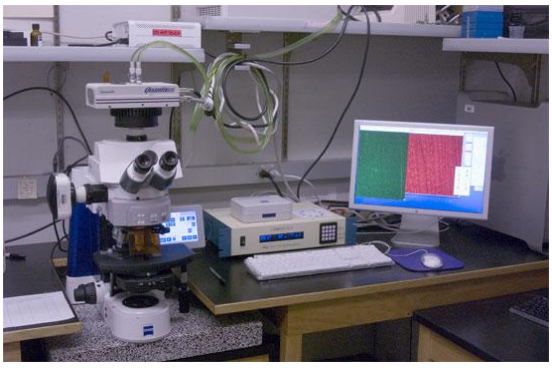

**Figure 10.** Axioimager M1 Fluorescent Microscope Set-up at the College of Natural Resources (CNR) in Berkeley.

The CNR website (microsopy.berkeley.edu) provides further details on the mechanism and capabilities of the fluorescent microscope system shown above. Experimental results/images

obtained from fluorescent density measurements are shown below. The area shown below is just that of the channel area, i.e. 110um*1mm (horizontal orientation), where the DNA is pipetted.

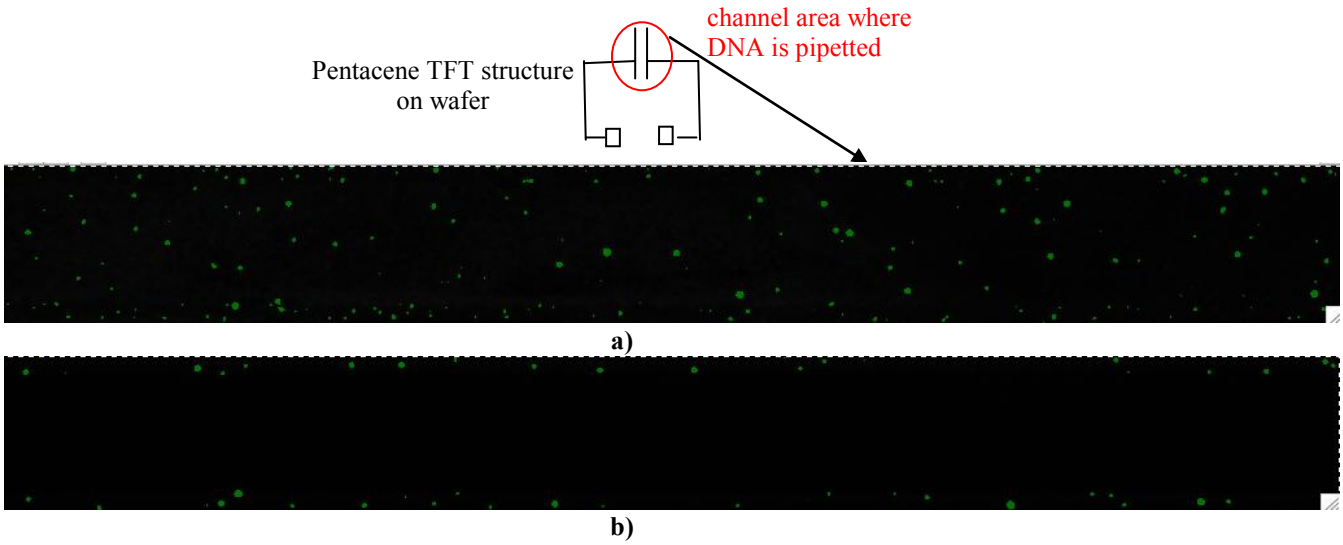


**Figure 11.** Fluorescent density images captured using the digital CCD camera in the fluorescent microscope system. The green dots in images a) and b), which are to represent green-fluorescent tagged DNA, are from 2 substrates with different pentacene thicknesses and concentrations of DNA.

The green dots seen above represent the green-fluorescent tagged DNA. The substrate in 11a, given the pentacene evaporation conditions that were used, is expected to have a rougher surface (referring to results shown in Section IV) than that of 11b. Correspondingly, more DNA can be seen immobilized in 11a. The quantitative measurement that was used to make this conclusion was fluorescent density measurements. Fluorescent density or intensity measurements were made using the camera, and its in-built segmentation software tool that adds up the intensity of different segments of green fluorescence within the imaged channel area. Before trying to correlate the these results with electrical results, control experiments were done to see if the fluorescent tag had any effects on the electrical characteristics. No-tag DNA and fluorescent tagged DNA were pipetted and treated with the same experimental protocol. Results showed that the fluorescent tag, by itself, causes no additional shift to the electrical characteristics.

While trying to correlate the electrical and visual results, some potential problems were discovered. After doing some control experiments on the pentacene surface, it was observed that the pentacene substrate also fluoresces, contributing its own fluorescent signal to the measurements above. This is to be expected of an organic semiconductor such as pentacene. Fluorescence occurs when a molecule, atom or nanostructure relaxes to its ground state after being electrically excited. State $S_0$ is called the ground state of the fluorophore (fluorescent molecule) and $S_1$ is its first (electronically) excited state [14].

A molecule in its excited state, $S_1$, can relax by various competing pathways. It can undergo non-radiative relaxation in which the excitation energy is dissipated as heat (vibrations) to the solvent. Excited organic molecules can also relax via conversion to a triplet state which may subsequently relax via phosphorescence or by a secondary non-radiative relaxation step. Relaxation of an $S_1$ state can also occur through interaction with a second molecule through fluorescence quenching. Finally, molecules that are excited through light absorption can transfer energy to a second 'sensitized' molecule, which is converted to its excited state and can then fluoresce [14]. The latter case is likely the cause of the fluorescent ‘noise’ that we are seeing with the measurements above. It is not easy to separate this from the actual signal unless the DNA is tagged with a fluorescent molecule which fluoresces at a wavelength that does not excite the pentacene molecule. Alternatives that are being considered will be discussed in the last paragraph of this section.

The second problem with fluorescent microscopy using the digital CCD camera is the resolution of the camera. The Max XY resolution of this fluorescent microscope is about 200nm. With the resolution of the available CCD camera, 100s of molecules needs to be clumped together in the 200nm space for the system to detect the fluorescent signal. As discovered

through AFM, the distribution of DNA on the surface is random. In other words, the DNA density in different scan areas is not expected to be consistent. Given the resolution of the digital CCD camera, the random distribution makes it difficult to accurately capture the amount of DNA on the surface.

To keep the pentacene substrate from fluorescing, different control experiments with a range of emission filters were tried on the surface. We were able to conclude that pentacene does not fluoresce at blue light wavelengths (450-495nm [15]) or below. In addition, to get as close as possible to the resolution of the Single Molecule Spectroscopy (SMS) [16], which would allow measurement of a single fluorescent molecule or a single strand of DNA, the College of Natural Resources at Berkeley has recently obtained a new EMCCD (electron-multiplying charge coupled device) camera, which is highly sensitive and super bright. It is much more sensitive than the camera that has been used so far.

Since results with the current system are promising, future experiments for correlation will be performed with blue fluorescent tagged DNA and the new EMCCD camera.

## B. Time-of-Flight Secondary Ion Mass Spectroscopy (TOF-SIMS)

This section covers the use of TOF-SIMS technique for correlation and the results obtains from the experiment.

### *i. Definition and Technical Capabilities*

Time-of-Flight Secondary Ion Mass Spectrometry (TOF-SIMS) is a surface analytical technique that focuses a pulsed beam of primary ions onto a sample surface, producing secondary ions in a sputtering process. Analyzing these secondary ions provides information about the

molecular and elemental species present on the surface. For example, if there were organic contaminants, such as oils adsorbed on the surface, TOF-SIMS would reveal this information, whereas other techniques may not. Since TOF-SIMS is a survey technique, all the elements in the periodic table, including H, are detected. Moreover, TOF-SIMS can provide mass spectral information, image information in the XY dimension across a sample, and also depth profile information on the Z dimension into a sample [17].

The surface sensitivity of TOF-SIMS makes it a good first pass at problem solving. Other techniques can be used to obtain in depth information. The imaging capabilities of TOF-SIMS can provide elemental and molecular information from defects and particles on the micron scale. TOF-SIMS can also be used for depth profiling and compliments dynamic SIMS. The advantages for TOF-SIMS for profiling are its small areas capabilities and also its ability to do survey depth profiles [17].

TOF-SIMS is known to be one of the most sensitive surface analytical techniques, with a detection limit of $10^7$- $10^{10}$ atoms/cm$^2$ sub-monolayer and a depth resolution of 2-3nm. It provides specific molecular information on thin (sub-monolayer) organic films/contaminants with an excellent detection limit (ppm) for most elements. The TOF-SIMS technique was used instead of SIMS because TOF-SIMS is able to perform the SIMS analysis on organic thin films and more specifically soft substrates. It is a non-destructive process tailored to work with soft substrates such as pentacene. TOF-SIMS has a few limitations. The samples that need to be analyzed must be vacuum compatible. In addition, this technique can be too surface sensitive with sample packaging; prior handling may also impact quality of results. Despite the limitations, the TOF-SIMS technique is extremely sensitive, reliable, and very useful in many applications.

### *ii. Experiment, Procedure, and Results*

The TOF-SIMS analysis was performed in the Evans Analytical Group labs in Sunnyvale, CA. The TOF-SIMS analysis was performed to get a visual proof of DNA on surface and to see if it is possible to correlate these results with the electrical measurements.

More specifically, the purpose of this analysis was to determine the relative levels of DNA on three samples: *Sample #1- Control:* Pentacene substrate with no buffer or DNA but which has gone through the same experimental protocol (fabrication and storage) as the other two; *Sample #2-Buffer:* Pentacene substrate with just pure buffer and NO DNA. The buffer, as discussed earlier is saline-sodium citrate solution; *Sample #3-DNA in buffer:* DNA was pipetted on the channel of the transistor. Note that all 3 samples were taken from the same substrate; each of the samples went through the same cleaning, evaporation, and storage procedures. The relative levels of DNA were assessed by monitoring the levels of sodium (Na) and phosphate ($PO_x$) ions.

***Experiment:***

Data was obtained using a gallium liquid metal ion gun (LMIG) primary ion source (Ion Potential: 12 kV for +ions and 18kV for –ions; DC Ion Current: 2nA). The instrument was operated in an ion microprobe mode in which the bunched, pulsed primary ion beam was rastered across the sample's surface. Three positive and three negative ion spectra were acquired from each sample in order to investigate the reproducibility of the data. Acquisition of multiple spectra serves to highlight possible chemical heterogeneity across the sample's surface. In each case the analytical area was 80μm × 80μm. Spectra were acquired by specifying a particular area of the sample as a "region of interest" (ROI). This allowed data to be acquired only from the channel, eliminating signal from the surrounding gold lines.

The elements of interest were $PO_x$ (for DNA) and Na (for buffer solution).

***Summary of Results:***

The highest levels of $PO_x$ and Na were observed on sample #3. These species were observed at significantly lower levels from sample #2. No $PO_x$ was observed from sample #1 which had the lowest levels of Na.

Other species observed from all samples included the pentacene substrate ($C_{22}H_{14}$), Polydimethylsiloxane (PDMS), which is a signal observed because of the hexamethyldisilazane (HMDS) layer in the dielectric/pentacene interface, and F, Fluorine.

***Discussion of Results:***

The results are presented as mass spectra, which are displayed as the number of secondary ions detected (Y-axis) versus the mass-to-charge (m/z) ratio of the ions (X-axis). The ion counts are shown on linear intensity scales, and probable empirical formulae for a number of peaks are identified in the figures. The multiple spectra obtained from each sample were generally very similar so only one representative spectrum from each sample in each polarity is included in this report. Mass Spectra results can be found in the appendix of this report.

The results are also presented as tables of normalized intensities. *These tables can be used to compare the level of a given species between samples; however, they cannot be used to compare the levels of different species either on the same sample or between samples.* This is because different species have different secondary ion yields so TOF-SIMS has different sensitivities for different species. The tables show the mean of three measurements and also the standard deviations.

| m/z | formula | 1, control | | 2, buffer | | 3, (DNA + buffer) | |
|---|---|---|---|---|---|---|---|
| | | *mean* | $\sigma$ | *mean* | $\sigma$ | *mean* | $\sigma$ |
| *Elements* | | | | | | | |
| 23 | Na | 16.1 | 6.0 | 569 | 146 | 4790 | 580 |
| 28 | Si | 3670 | 180 | 3610 | 160 | 587 | 38 |
| *Pentacene* | | | | | | | |
| 278 | $C_{22}H_{14}$ | 105 | 11 | 40.4 | 7.7 | 55.0 | 6.2 |
| *PDMS* | | | | | | | |
| 73 | $C_3H_9Si$ | 408 | 31 | 317 | 42 | 95.9 | 12.0 |
| 147 | $C_5H_{15}Si_2O$ | 16.5 | 5.6 | 73.1 | 13.0 | 15.6 | 1.7 |

**Table 1.** Normalized positive ions of interest
(normalized relative to total ion counts ×10000)

Table 1 above presents the normalized intensities of the positive ions of interest. Elemental species observed from all three samples included Na, Si, and F. The levels of Na varied significantly among the samples with the highest levels observed from sample #3 and the lowest levels on Sample #1. The highest levels are expected from sample #3 because the DNA molecules themselves will have the buffer solution (Na) attached to them. Sample #1 most likely has Na because of contaminants from the environment. Comparable levels of Si were observed on samples #1 and #2 while lower levels were found on #3. The lower levels in sample #3 are possibly due to the strong signal exhibited by the Na in this sample. This can also be observed in the mass spectra included in the appendix of this report.

| m/z | formula | 1, control | | 2, buffer | | 3, DNA + buffer) | |
|---|---|---|---|---|---|---|---|
| | | *mean* | $\sigma$ | *mean* | $\sigma$ | *mean* | $\sigma$ |
| 47 | PO | nd | - | 0.337 | 0.018 | 0.551 | 0.150 |
| 63 | $PO_2$ | nd | - | 0.295 | 0.022 | 2.91 | 0.81 |
| 79 | $PO_3$ | nd | - | nd | - | 2.45 | 0.73 |

"nd" indicates species not detected on that sample

**Table 2.** Normalized negative ions of interest
(normalized relative to total ion counts ×10000)

Table 2 above presents the normalized intensities of the negative ions of interest. The focus was on the $PO_x$ ions to determine the presence of DNA on the surface and the relative amounts of DNA on the different samples. Phosphate ions ($PO_x$) were observed in negative polarity only on samples #2, and #3. The levels of $PO_x$ on sample #3 were significantly higher than those observed from sample #2. The $PO_3^-$ ion in particular was observed only on sample #3. Phosphate ions were not clearly observed in the mass spectra (shown in appendix) due to the many strong hydrocarbons in the spectra.

Many ions due to HMDS (shown as PDMS in the mass spectra and tables) were observed from all samples. Several hydrocarbon ions were also observed from all samples, and these are shown in the mass spectra included in the appendix. Representative low mass positive ions include $C_2H_3$, $C_3H_5$, and $C_4H_7$. Representative negative ions include $C_2H$, $C_4H$, and $C_6H$. Species such as these have multiple possible sources. They may be adsorbed low mass molecular species or they may be fragment ions from other higher mass molecular species. The parent molecule of the pentacene substrate ($C_{22}H_{14}$, m/z 278) was clearly observed on all samples. This indicates that the coverage of adsorbed species (e.g. DNA and HMDS) is discontinuous and/or less than a monolayer thick.

TOF-SIMS analysis has shown the presence of phosphate groups, particular $PO_2$ and $PO_3$ (from DNA) and sodium (from buffer solution) in highest concentrations in sample #3, the sample with DNA immobilized in the channel. The control sample (sample #1) shows small traces of sodium and the buffer sample (sample #2) shows small traces of PO possibly due to environment contribution and/or contamination. Since Sample #3 has shown significantly higher amounts of the species of interest, the presence of DNA on the pentacene surface has been confirmed.

Fluorescent Microscopy and TOF-SIMS have both shown useful results to ascertain the physical origins of electrical transduction behavior. TOF-SIMS results have confirmed the presence of DNA on pentacene surface while modified fluorescent microscopy measurements have shown potential for use in directly correlating the amount of DNA immobilized on the surface with the shift of the electrical performance characteristics.

# IV. Optimization of DNA Immobilization and Sensor Sensitivity

DNA immobilization has been previously discussed in Section II of this report. Physical absorptive immobilization, the mechanism through which DNA immobilizes on pentacene, highlights the importance of the topology of the pentacene film surface for immobilization of DNA and the sensitivity of the sensor. DNA is known to segregate to topological features on pentacene surface. We are able to exploit the control of pentacene evaporation conditions to tune pentacene film morphology to maximize sensitivity. In this section, we demonstrate DNA detection using optimized films.

The optimization experiment is split up into two parts. The first is a set of experiments that characterize the pentacene (vary the pentacene morphology) by varying the input parameters. The second integrates the DNA into the experiments, thereby arriving at the best surface and evaporation conditions for highest sensor sensitivity.

## A. Pentacene Characterization Experiment

By carefully controlling input parameters to set different evaporation conditions, we analyze pentacene morphological and electrical characteristics. The input parameters that were varied and the outputs that were extracted are shown in Table 3 below.

| **Input Variables** | **Output Characteristics** |
|---|---|
| Thickness of Pentacene film<br>Input Current (Temperature of the crucible)<br>Substrate Temperature | $I_{dsat}$ (Saturation Current)<br>Mean Roughness<br>Grain Size<br>Evaporation Rate<br>Coverage Area |

**Table 3.** Input and Outputs for Pentacene Characterization Experiment.

*i. Experimental Setup: Response Surface Design of Experiments (DOE)*

Because the goal of this part of the experiment was to relate the input and output parameters, the experiment needed to be tailored to ultimately result in providing these relationships. To perform this comprehensive analysis, design of experiments (DOE) set-up was used. In particular, a surface response DOE was used because of the importance of gaining a thorough understanding of the output characteristics for optimizing DNA immobilization.

The DOE set-up was configured using JMP, a statistical software. The DOE platform in JMP is an environment for describing the factors, responses and other specifications, creating a designed experiment. JMP allows the design of different types of DOE including screening design and response surface design. The former is to get an overall understanding while the latter is gain an in-depth understanding of the relationships between input and output parameters.

Response surface designs are useful for modeling a curved surface (quadratic) to continuous factors. If a minimum or maximum response exists inside the factor region, a response surface model can pinpoint it. Three distinct values for each factor are necessary to fit a quadratic function, so the standard two-level designs (such as screening design) cannot fit curved surfaces. The most popular response surface design is the central composite design, illustrated by Figure 12 below [19].

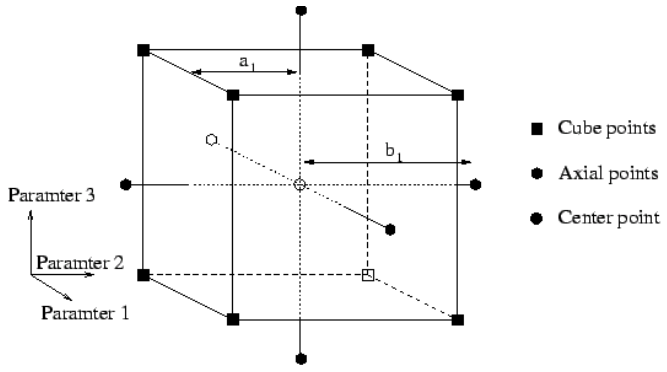


**Figure 12.** Central Composite Design Methodology [18].

CCD combines a two-level fractional factorial (used in screening designs) and two other kinds of points, namely c*enter points*, for which all the factor values are at the zero (or midrange) value and *axial* (o*r star*) *points*, for which all but one factor are set at zero (midrange) and that one factor is set at outer (axial) values. There are two main types of central composite designs, namely uniform precision and orthogonal designs. The properties of these central composite designs relate to the number of center points in the design and to the axial values. For orthogonal designs, the number of center points is chosen so that the second order parameter estimates are minimally correlated with the other parameter estimates. Uniform precision, which was used for the following DOE, means that the number of center points is chosen so that the prediction variance at the center is approximately the same as at the design vertices [19].

Using a surface response design and more specifically, a uniform precision CCD set up, the DOE shown in Table 4 below was followed. A set of 17 evaporation conditions was designed for the experiment.

| | Pattern | Thickness of Pentacene | Substrate Temp | Input Current | Idsat | Grain Size | Mean Roughness | Evaporation Rate | Coverage Area |
|---|---|---|---|---|---|---|---|---|---|
| 1 | -++ | 140.54 | 60.878 | 5.249 | • | • | • | • | • |
| 2 | 00A | 200 | 47.5 | 5.35058713 | • | • | • | • | • |
| 3 | 000 | 200 | 47.5 | 5.1 | • | • | • | • | • |
| 4 | +++ | 259.46 | 60.878 | 5.249 | • | • | • | • | • |
| 5 | ++- | 259.46 | 60.878 | 4.951 | • | • | • | • | • |
| 6 | +-- | 259.46 | 34.122 | 4.951 | • | • | • | • | • |
| 7 | 0A0 | 200 | 69.9990245 | 5.1 | • | • | • | • | • |
| 8 | 0a0 | 200 | 25.0009755 | 5.1 | • | • | • | • | • |
| 9 | A00 | 299.999402 | 47.5 | 5.1 | • | • | • | • | • |
| 10 | 000 | 200 | 47.5 | 5.1 | • | • | • | • | • |
| 11 | --+ | 140.54 | 34.122 | 5.249 | • | • | • | • | • |
| 12 | -+- | 140.54 | 60.878 | 4.951 | • | • | • | • | • |
| 13 | +-+ | 259.46 | 34.122 | 5.249 | • | • | • | • | • |
| 14 | --- | 140.54 | 34.122 | 4.951 | • | • | • | • | • |
| 15 | 000 | 200 | 47.5 | 5.1 | • | • | • | • | • |
| 16 | a00 | 100.000598 | 47.5 | 5.1 | • | • | • | • | • |
| 17 | 00a | 200 | 47.5 | 4.84941287 | • | • | • | • | • |

**Table 4.** JMP Surface Response DOE for Pentacene Characterization Experiment.

The input variables are shown in columns 3, 4, and 5. The output characteristics are in columns 6-10. For the DNA immobilization part of this experiment, 2 or 3 more columns will be added, namely $I_{dsat}$ ratio, Threshold Voltage ($V_t$) shift, and mobility shift.

A set of 9 points was measured within each of these experiments in order to study the variation within wafer and wafer to wafer variation. The measurement setup used for each of the 17 experiments is shown in Figure 13 below.

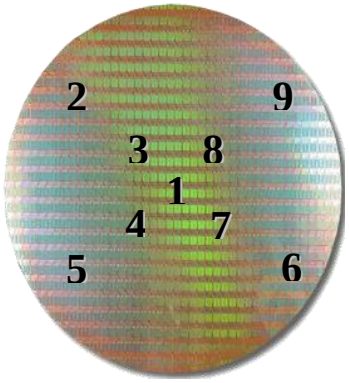


**Figure 13.** A set of 9 points was measured for each of the 17 experiments in the DOE to study variation within the wafer and wafer-to-wafer variation.

### *ii. Experiment Protocol*

The experimental procedure and specifications for the pentacene characterization experiment is discussed below:

1) N++ silicon as substrate
2) 1000Å wet oxidation for $SiO_2$ (using Tystar oxidation furnace)
3) HMDS on $SiO_2$ surface (to optimize the interface between hydrophobic (photoresist) and hydrophilic ($SiO_2$) surfaces)
4) Photoresist spinning followed by lithography to define source and drain contacts
5) Evaporation of 1000Å of gold for source and drain contacts
6) Lift-off for 45 minutes in acetone

7) Sonication/Cleaning of Substrate- another 45 minutes in acetone followed by 45 minutes in IPA (isopropyl alcohol)
8) HMDS on surface (to optimize interface between $SiO_2$ (hydrophilic) and pentacene(hydrophobic))
9) Evaporation of Pentacene using the specified input parameters on the DOE (the pentacene evaporation was performed under vacuum with a chamber pressure of ~2.2 x$10^{-7}$ Torr)

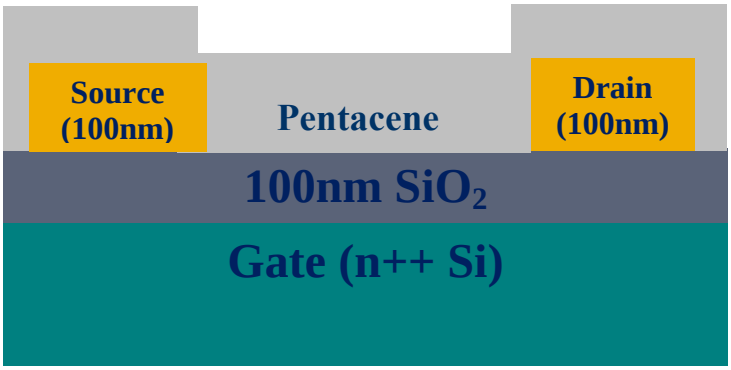


**Figure 14.** Pentacene TFT structure.

The sonication/cleaning step (step 7) is especially important for sensor sensitivity since this establishes the interface between the dielectric and the semiconductor. DNA immobilizes and interacts very close to this interface to cause the shift in the transistor characteristics.

*ii. Results*

***Results: Within Wafer and Wafer to Wafer Variation***

The results shown in Figure 15 below highlight the variation within each experiment and across the different experiments. In addition, the wide range of electrical characteristics across the DOE further emphasizes the importance of controlling these evaporation conditions to determine the optimum immobilization for highest sensor sensitivity. The x axis of the graph corresponds with the experiments on the DOE in Table 4.

The output shown here is saturation current ($I_{dsat}$). The variation within each wafer and from wafer to wafer will have a direct correlation with the other output characteristics. If there's more variation (bigger standard deviation) within one experiment, then this is a result of lack of uniformity of the pentacene surface in that experiment. This relates back to the morphological characteristics. For example, higher input current or thicker pentacene, depending on which factor dominates, likely causes non-uniform morphology within a wafer, increasing the variation in electrical performance. This will be further discussed in the next part of this section.

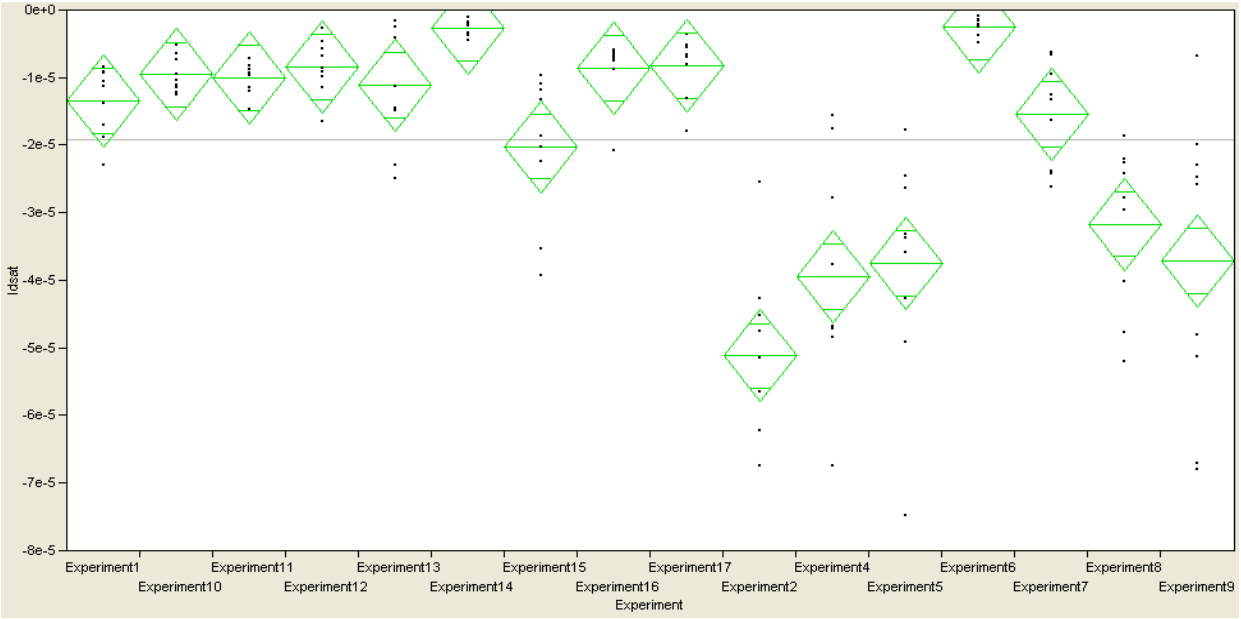


**Figure 15.** $I_{dsat}$ (electrical characteristics) for all 17 experiments. These results display the different performance characteristics across the DOE as well as the variation across the experiments.

The green diamonds seen in Figure 15 do not represent standard deviation. A means diamond illustrates a sample mean and 95% confidence interval, as shown in Figure 16 below.

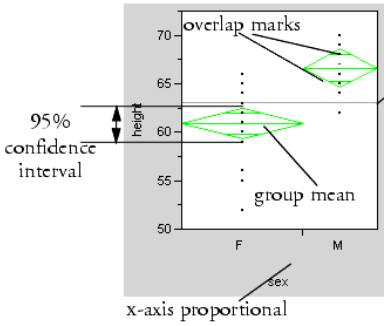


**Figure 16.** Explanation of the t-test mean diamonds used for statistical purposes [19].

The line across each diamond represents the group mean. The vertical span of each diamond represents the 95% confidence interval for each group. Overlap marks are drawn above and below the group mean. For groups with equal sample sizes, overlapping marks indicate that the two group means are not significantly different at the 95% confidence level. The confidence interval computation assumes that variances are equal across observations. Therefore, the height of the confidence interval (diamond) is proportional to the reciprocal of the square root of the number of observations in the group [19].

The horizontal extent of each group along the *x*-axis (the horizontal size of the diamond) is proportional to the sample size of each level of the *x* variable. It follows that the narrower diamonds are usually the taller ones because fewer data points yield a less precise estimate of the group mean [19]. The t-test/anova analysis shown in Figure 15 also shows the sameness data. Between two experiments, if the overlap/sameness value (measured by t-test) is <5%, then we can be 'confident' that they are statistically different.

The variation can be characterized by the standard deviation value for each of the experiments. Experiment 9 had the highest standard deviation value of 0.000022, and the corresponding variation can be seen clearly in Figure 15. Experiment 14 and Experiment 6, had the lowest variation with a standard deviation of 0.000001.

## *Results: Relating Input and Output Parameters*

### 1. Saturation Current ($I_{dsat}$)

Figure 18 below shows the effect that the three input parameters (Input Current, Thickness of Pentacene, and Substrate Temperature) have on Saturation current ($I_{dsat}$). Saturation current and other electrical characteristics were measured using the Agilent HP4156 probe station purged in

nitrogen. The measurements were done under nitrogen, as is usually the practice when measuring pentacene transistors, because pentacene is oxygen-sensitive.

Figures 17 and 19 are extracted by JMP using the 153 experimental/electrical measurements (17 experiments * 9 measurements for each) performed. Using leverage plots, some of which are shown in Figure 17 below, and relating the input parameters to outputs, JMP is able to provide a relationship between the input and output characteristics, which are shown in Figures 17 and 19.

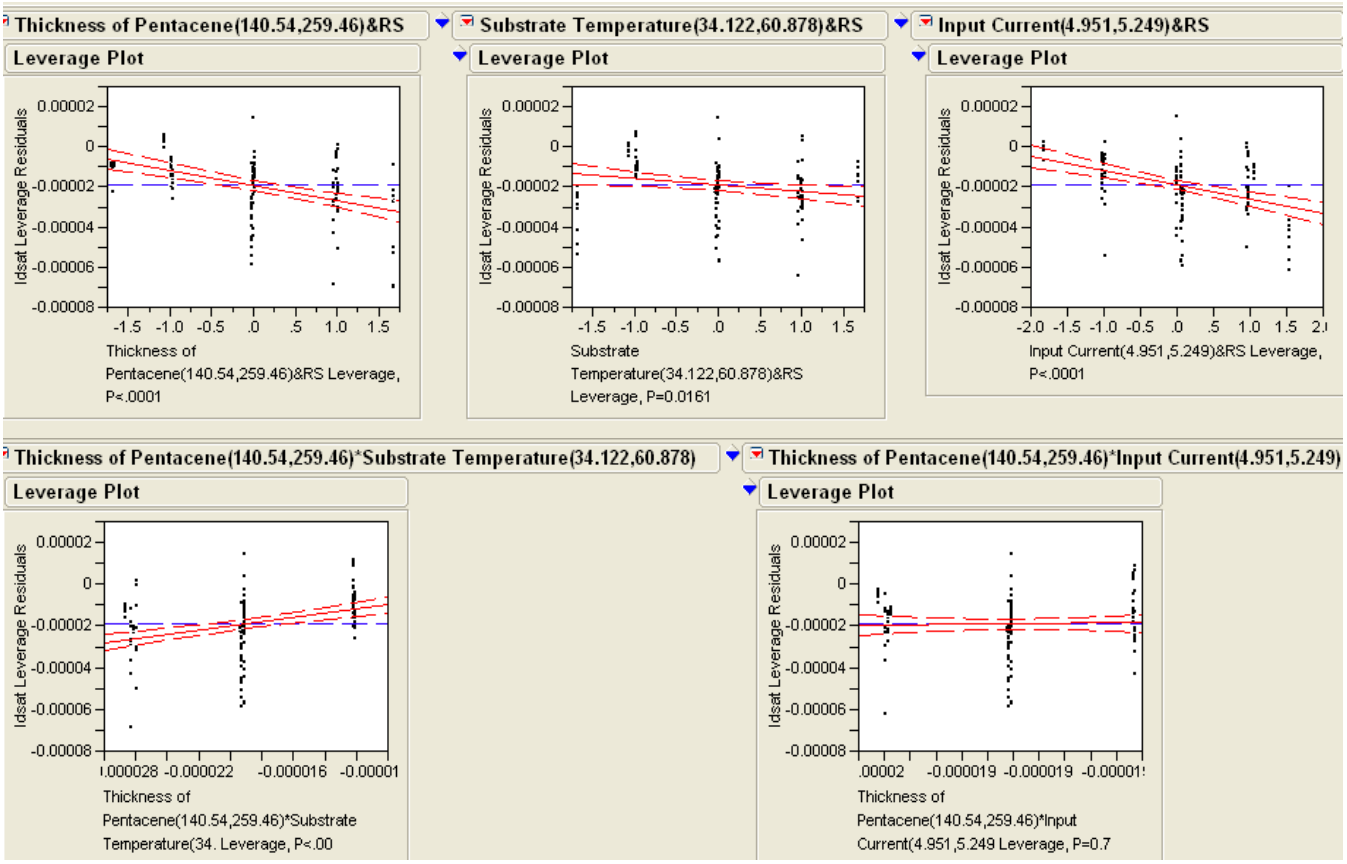


**Figure 17.** Leverage Plots relating input and output parameters using the measurements performed. Some parameters show a cause-effect relationship while others do not affect the saturation current.

Figure 18 below shows how the three input parameters independently affect the saturation current.

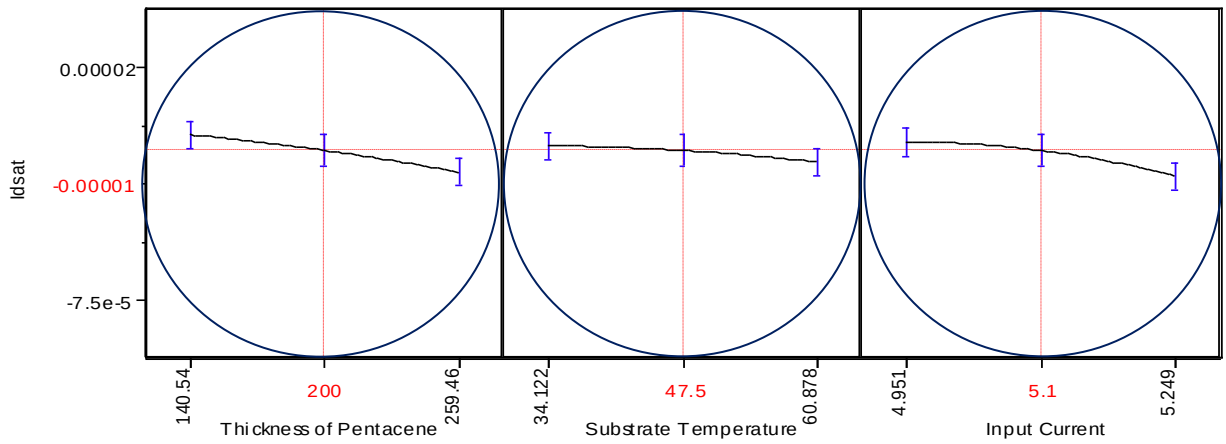


**Figure 18.** Relationship between the input parameters and $I_{dsat}$.

As mentioned earlier, the pentacene TFT device is a p-type accumulation device; the Y-axis in the figure above is negative current representing hole current. The figure above shows that as the thickness of the pentacene increases, the hole current (magnitude) also increases. This result can be justified using a schematic of the known growth modes of pentacene shown in Figure 19. The stacking of the pentacene and surface coverage causes this increase in electrical characteristics. Figure 19 below shows the schematic diagram of the pentacene throughout a range of thicknesses, and its effect on the electrical characteristics is further explained below.

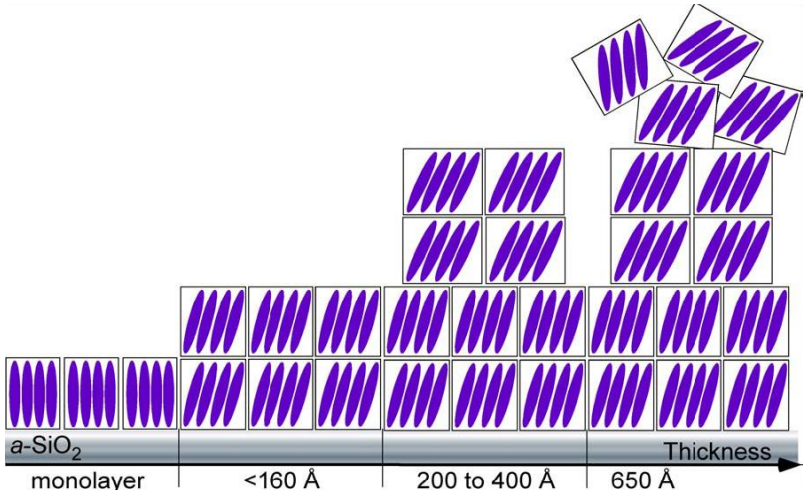


**Figure 19.** Schematic diagram depicting the phases and grain orientation in various pentacene film [20].

The schematic diagram shown above has been produced as a result of GIXD (grazing incidence X-ray diffraction) characterization done by Dr. Sandra Fritz [20]. The schematic diagram shows

that after about 400 Å, the pentacene starts exhibiting 'bulk-like' characteristics. 200-400 Å represents the transition. The increase in current in our experiment is mainly due to the stacking of the monolayers and uniform coverage till about 200 Å or so. In our experiment, the thicknesses were varied from 100-300 Å. Throughout this range, the stacking helps increase the mobility and conductivity. The coverage starts getting worse after about 400 Å.

The results in Figure 18 also show that as the substrate temperature increases, the saturation current increases. As the substrate temperature increases, the grain size increases due to thermodynamic factors such as sticking coefficient and diffusion of the pentacene grains during evaporation. As many groups have shown, as grain size increases, the mobility increases. Since electrical conductivity is limited by charge transfer across grain boundaries the formation of larger crystallites leads to enhanced conductivities [23]. Mobility increase leads to the current increase that we see in our experiment.

Increase in input current, which directly relates to the temperature of the crucible holding the pentacene, interestingly increases the overall saturation current as well. An interplay of multiple factors is most likely causing this shift.

The interplay among the different factors is shown in the interaction plot shown in Figure 20. When the lines within an interaction box are not parallel, it indicates that the two inputs corresponding to the 'interaction' box are dependent on each other in causing an effect on the output, which in this case in $I_{dsat}$. Note that Figure 18 delineates how the inputs are independently affecting $I_{dsat}$ while Figure 20 presents the dependent relationships. In Figure 20 below, the two factors that are interacting in affecting $I_{dsat}$ are thickness of pentacene and substrate temperature. These are circled in the figure below.

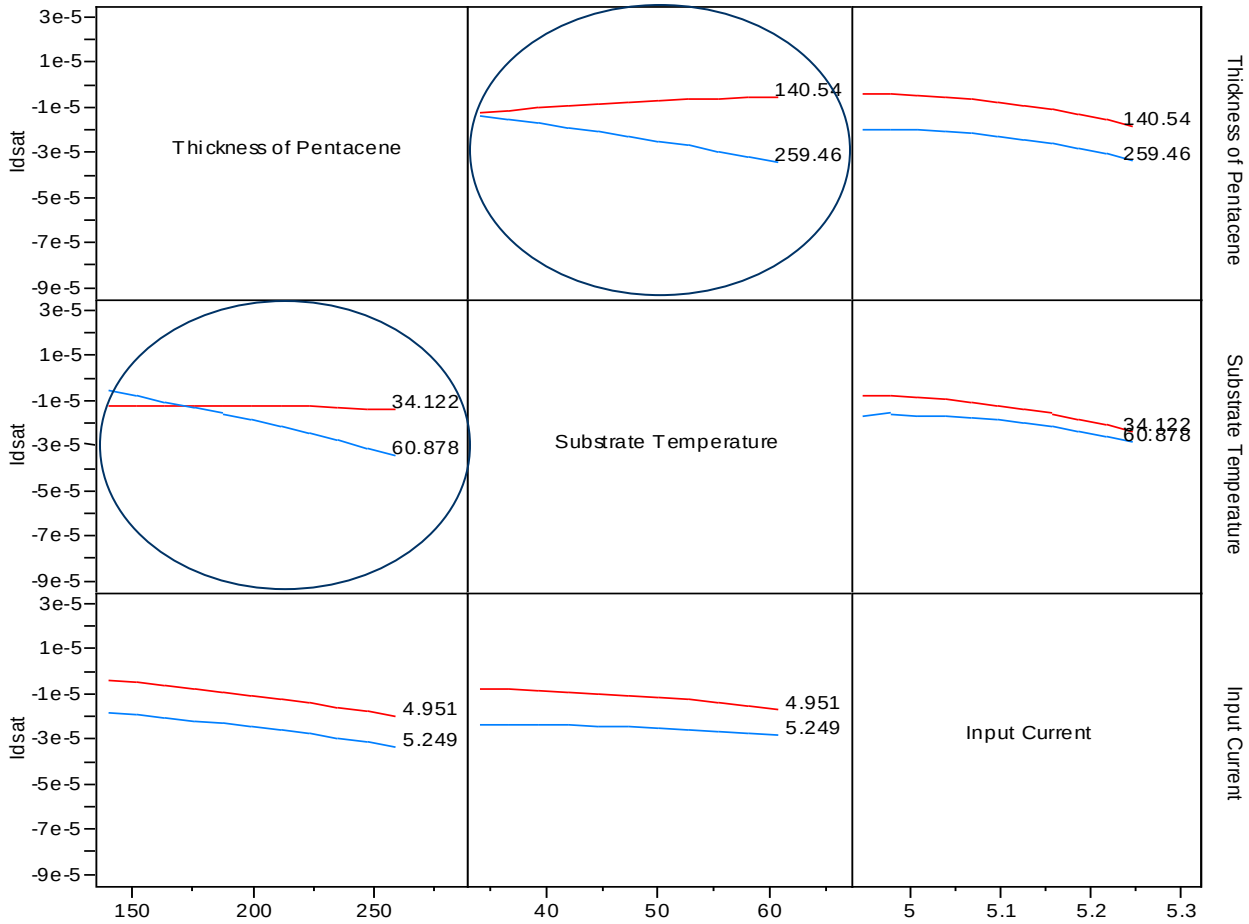


**Figure 20**. Interaction Profiler Plot for $I_{dsat}$.

In Figure 18, the values of the inputs were set at midpoint to get the general trend. The interaction plot reveals that since thickness of pentacene and substrate temperature are interacting, if the thickness of pentacene for example changed from the midpoint value of 200 Å to 100 Å, then the way the substrate temperature affects the $I_{dsat}$ will be different (i.e. different slope). An illustration of this is shown in Figure 21 below. When tuning the output characteristics, these interactions need to be taken into consideration as well.

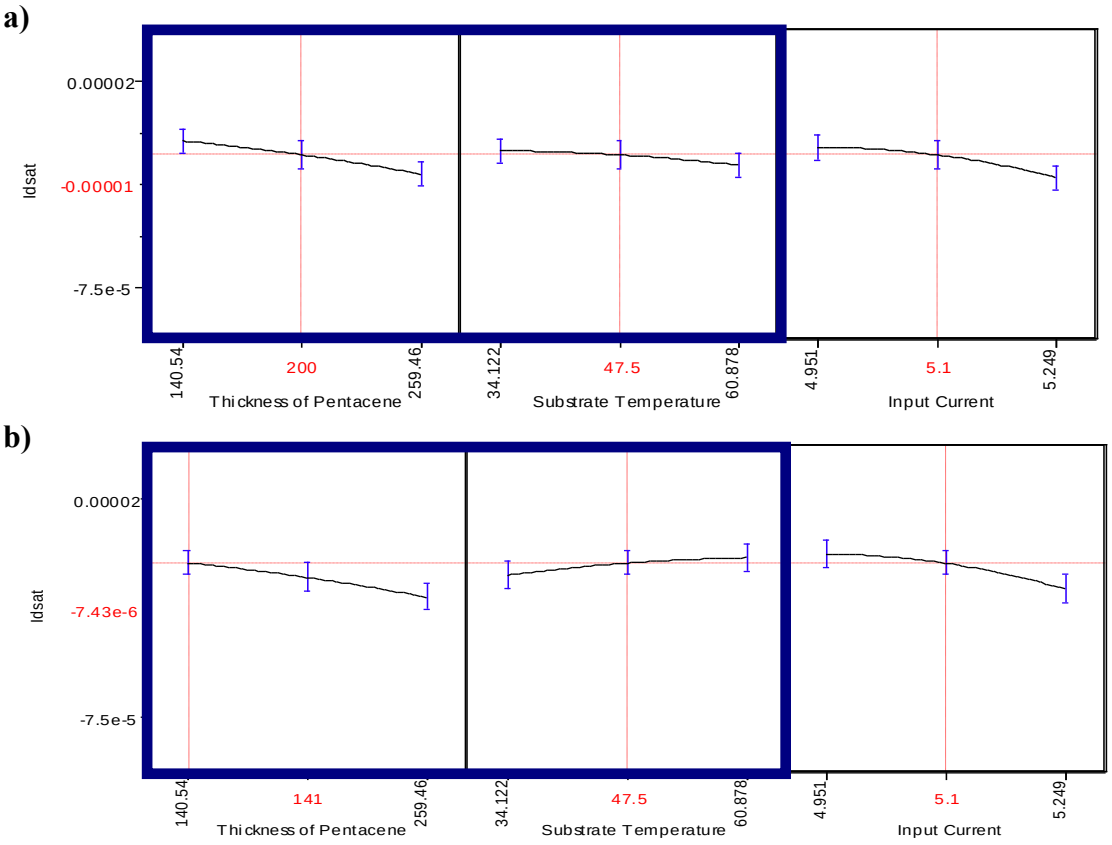


**Figure 21.** Illustration of the significance of the interaction plot.

Note that in Figure 21b, the thickness of pentacene has been set at 141 Å (i.e. the middle red line has been moved). In this case the substrate temperature has the opposite effect on $I_{dsat}$ as compared to Figure 21a. The reason for the interaction here can be supported by the explanations that have been already provided on how the thickness of pentacene affects the stacking and consequently the saturation current.

Figure 22 shows the wide range of electrical characteristics obtained by varying the evaporation conditions. The saturation current varied from about ~2 $\mu$A in the lowest performing sample to ~60 $\mu$A on the highest performing sample. Figure 22 below shows the characteristics from two different experiments, representing the lowest and highest performance.

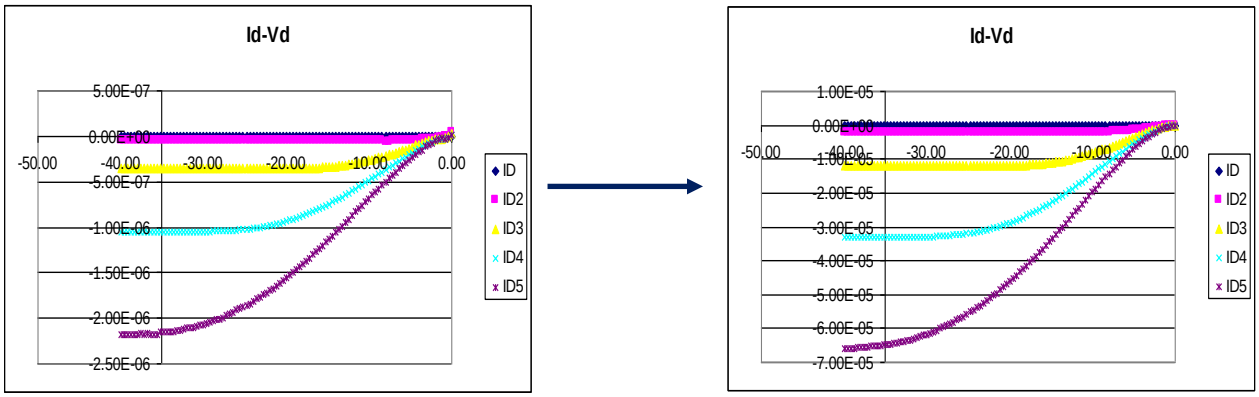


**Figure 22.** $I_d$- $V_d$ characteristics from 2 different experiments with the lowest(left) and highest(right) performing samples.

To summarize, the three input factors affect the $I_{dsat}$ in the following way. Increase in thickness of pentacene causes an increase in the hole current because of the increase in film stacking and coverage explained using the schematic diagram. The increase in substrate temperature leads to bigger grain sizes, which consequently causes the enhanced conductivity. Finally, the input current increase also enhances the performance because of a combination of an increase in grain size and interplay with the other input factors.

## 2. Mean Roughness of Pentacene Film Surface

Using a similar system of leverage plots as shown in Figure 17, the relationship between the input factors and mean roughness has been extracted and shown in Figure 23. Mean roughness was measured using Atomic Force Microscopy (AFM).

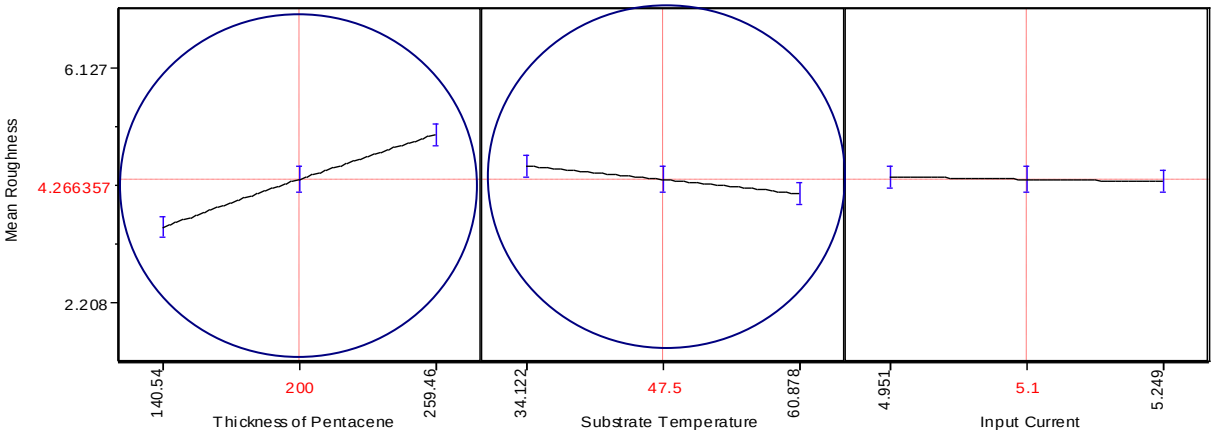


**Figure 23.** Relationship between the input parameters and mean roughness.

As the thickness of pentacene increases, the film roughness increases because the higher the number of monolayers, the rougher the film usually tends to be. This is further confirmed when looking at the schematic diagram in Figure 19. As the thickness of the pentacene film increases, the stacking becomes misaligned, especially after about 160 Å or so. Despite the increase in roughness, the current has still gone up with higher thickness possibly because other factors that affect the current such as better transport within a monolayer dominated.

As the substrate temperature increases, the roughness decreases. When evaporation of pentacene is done at higher substrate temperatures, the formation of the pentacene crystals on the surface is more ordered, thereby reducing the overall roughness. The effect of substrate temperature on the ordering of thin films of pentacene has been analyzed previously [24].

The input current does not independently affect the mean roughness according to Figure 23 above, but it does interact with both substrate temperature and to a lesser extent, thickness of pentacene as shown in Figure 24 below. Although at a pentacene thickness of 200 Å and a substrate temperature of $47.5\,°C$, the input current does not affect the mean roughness, at other values of thicknesses and substrate temperatures, it does. Depending on what thickness and substrate temperature turns out to be ideal for DNA immobilization and overall sensitivity, the input current will have to be tuned accordingly.

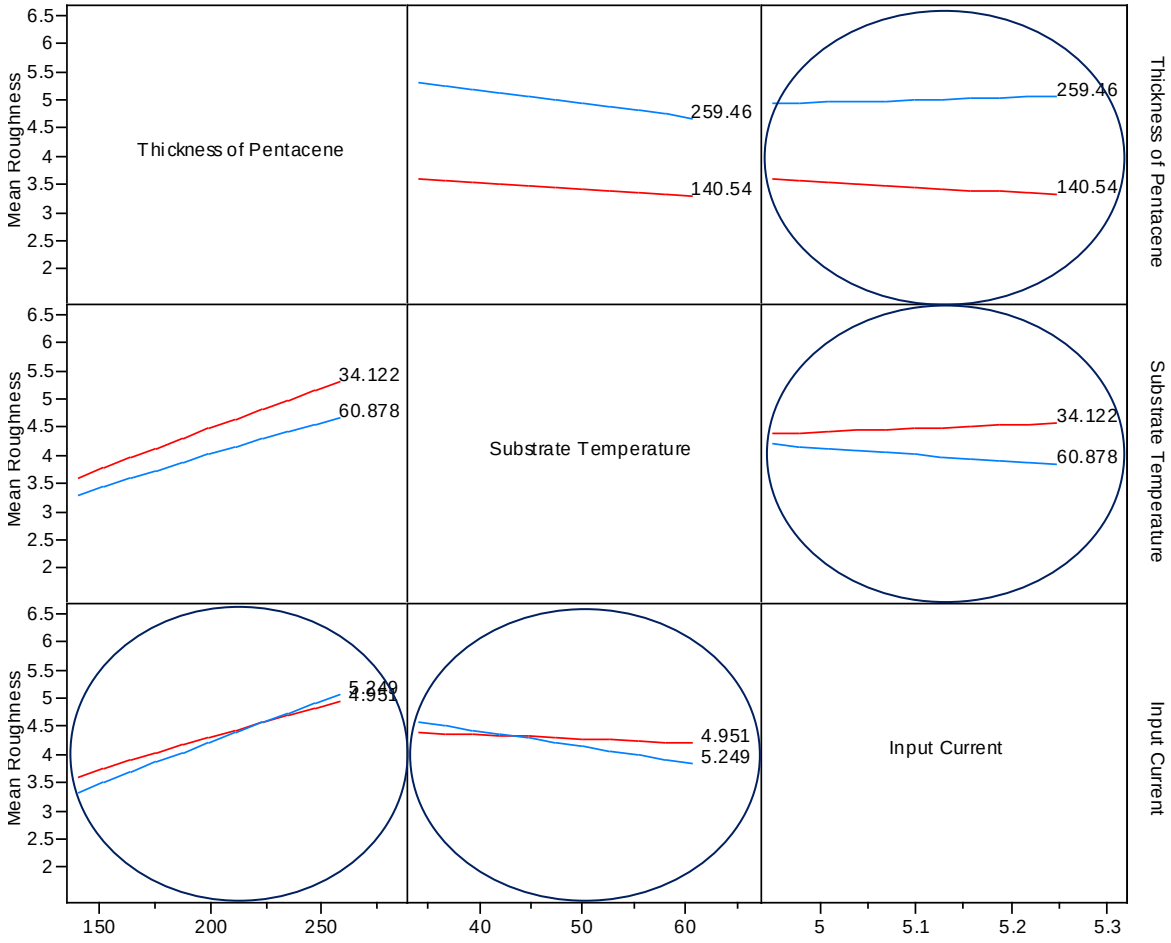


**Figure 24.** Interaction Profiler Plot for Mean Roughness.

As previously discussed, the topological features on the pentacene film are critical for DNA immobilization and sensor sensitivity. By doing AFM on these samples, surface roughness data on the samples were extracted. Figure 25 shows AFM images of samples from 2 different experiments, representing surfaces with the lowest (2.208nm) and highest (6.127nm) mean roughness. The wide range of the surface roughness data further emphasizes the need and importance of controlling the input parameters to get optimum morphological conditions for highest sensitivity.

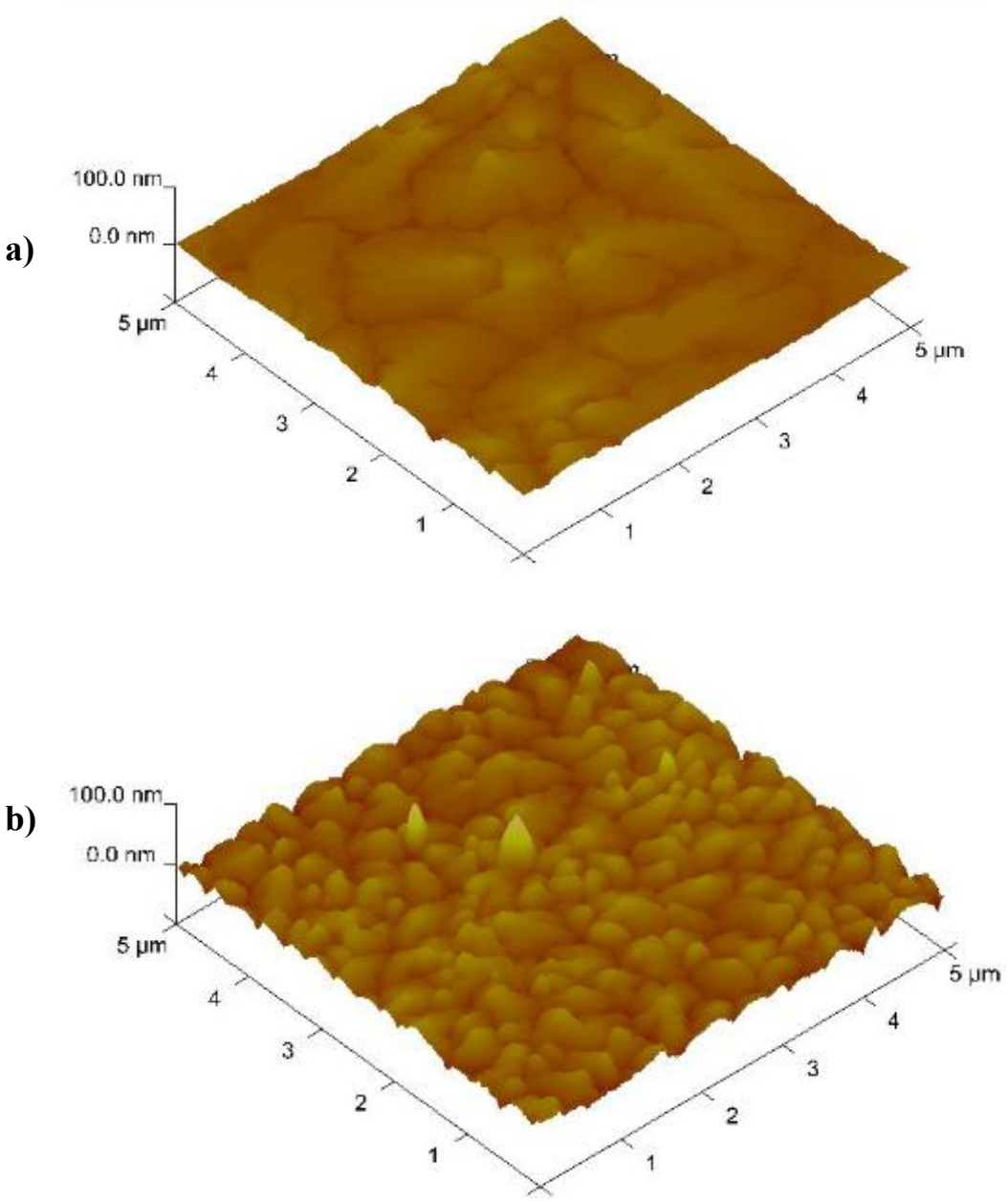


**Figure 25.** AFM images of samples from 2 different experiments with the lowest (a) and highest (b) surface roughness parameters. The lowest extracted roughness value was 2.208nm while the highest was 6.127nm.

### 3. Pentacene Grain Size

Grain boundaries are important topological features where DNA can immobilize. Therefore, grain size is an important parameter to characterize. Atomic Force Microscopy (AFM) was used to measure grain size. After extracting AFM images from tapping mode scans, the grain size was measured by boxing the area around an average-size grain in a particular scan.

Keeping the systematic variation in consideration, this measurement technique is valid to make a general comparison across the different experiments. Figure 26 below, a derivation from the leverage plots discussed earlier, shows how the input parameters affect the grain size.

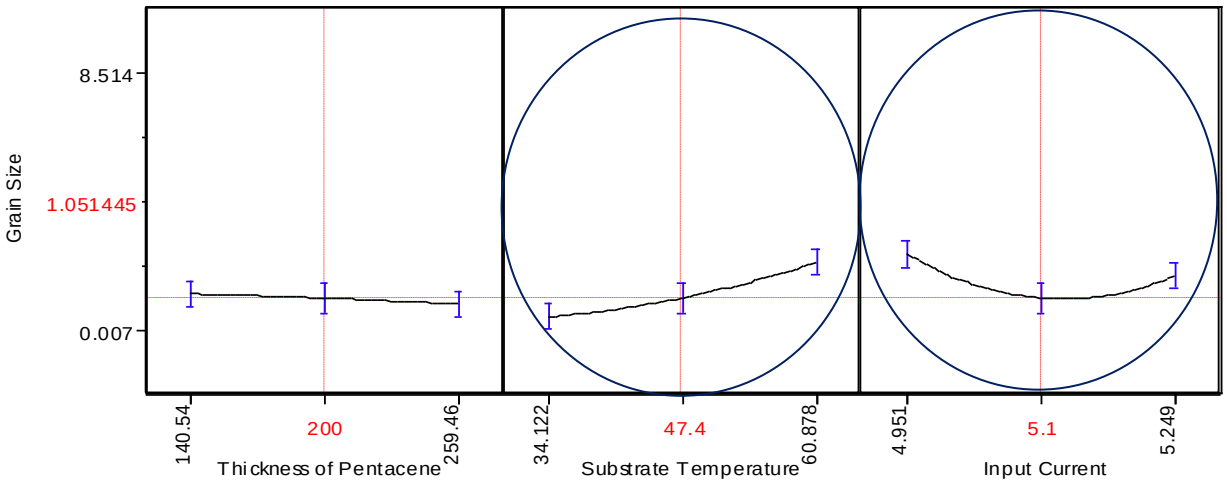


**Figure 26.** Relationship between the input parameters and grain size.

To begin with, the thickness of pentacene, as expected, does not affect the grain size. This is true in Figure 26 above as well as in the interactive profile shown below in Figure 27. As substrate temperature increases, the grain size also increases (which in turn leads to better electrical performance). The increase in grain size can be attributed to Oswaldt Ripening effects [25]. Oswaldt Ripening is an observed phenomenon in solid (or liquid) solutions which describes the evolution of an inhomogeneous structure over time. When a phase precipitates out of a solid, energetic factors will cause large precipitates to grow, drawing material from the smaller precipitates, which shrink. With higher substrate temperature, this thermodynamically-driven spontaneous process occurs because larger particles are more energetically favored than smaller particles. This stems from the fact that molecules on the surface of a particle are energetically less stable than the ones already well ordered and packed in the interior. Large particles, with their lower surface to volume ratio, results in a lower energy state (and have a lower surface

energy). As the system tries to lower its overall energy, molecules on the surface of a small (energetically unfavorable) particle will tend to diffuse through solution and add to the surface of larger particle. Therefore, the smaller particles continue to shrink, while larger particles continue to grow [27], leading to the larger grain size with higher substrate temperatures.

The input current shows an interesting non-linear relationship with grain size. The expected relationship here would be that as input current decreases, the grain size would increase linearly because of the way the grains are formed. When the pentacene crystals hit the substrate as they are being evaporated, they grow till they hit another crystal around them. With lower evaporation rate, the crystals have 'time' to grow bigger on the surface. This linear relationship is not seen because of two possible reasons. One is that there are more factors/variables interacting that we are not aware of and/or we will see in the interaction plot below. The other reason could be the way the grain size was measured. Since the grain size was measured as an average measurement from sample to sample in AFM, a more precise way of measuring the grain size may need to be implemented to get a clearer relationship between input current and grain size.

Figure 27 addresses the interaction among the different parameters. The main interaction happens between substrate temperature and input current, which might help better explain the non-linear relationship being seen between input current and grain size.

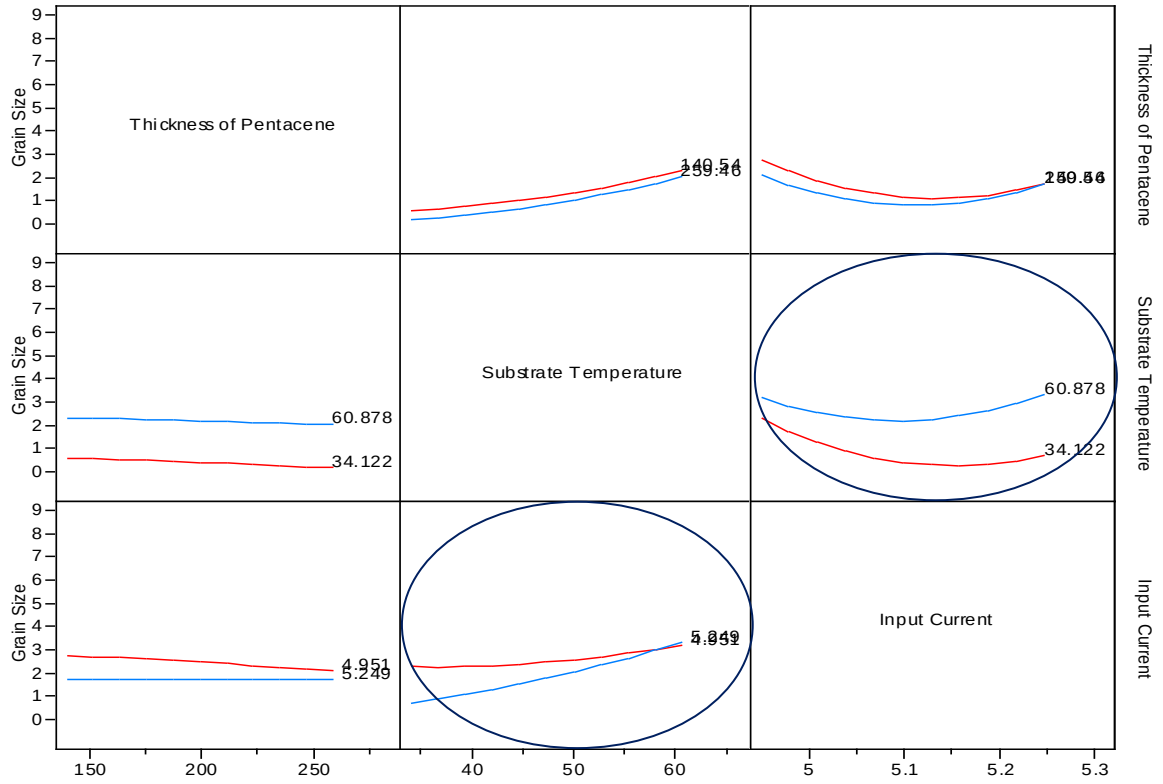


**Figure 27.** Interaction Profiler Plot for Grain Size.

Again, since grain size and grain boundaries are an important part of sensitivity of our sensor, the range of our grain size from 8.514 $\mu$m$^2$ down to 0.314 $\mu$m$^2$, illustrated in Figure 28, emphasizes the importance of tuning the morphology to suit the necessary conditions for DNA interaction. This will be discussed in depth in the following sections.

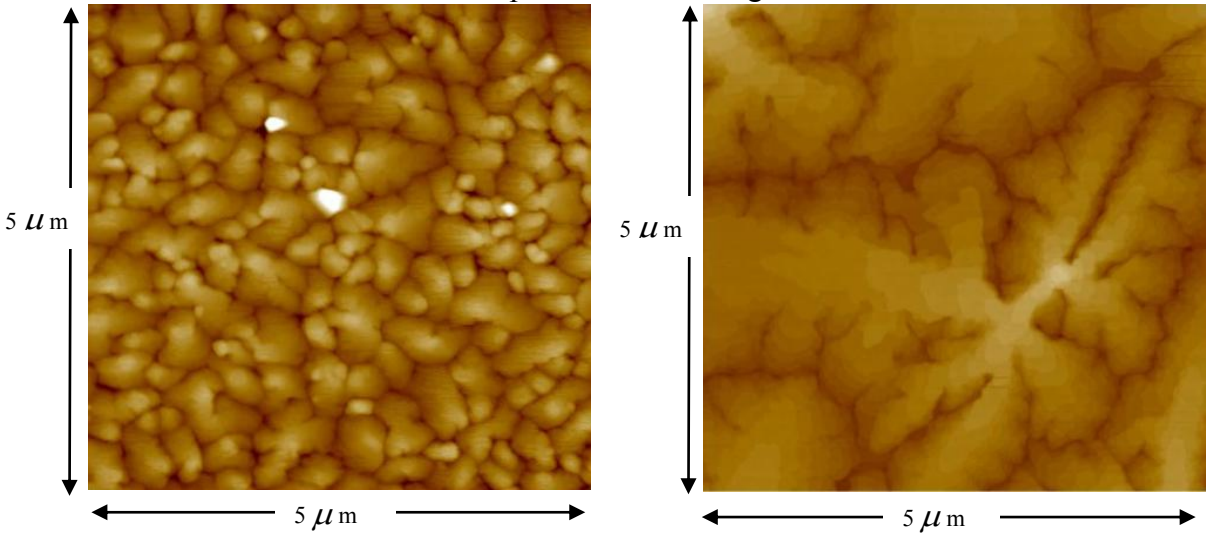


**Figure 28.** AFM images of samples from 2 different experiments consisting of the smallest grain size (left) of 0.314 $\mu$m$^2$ and the biggest grain size (right) of 8.514 $\mu$m$^2$.

**4 & 5. Evaporation Rate and Coverage Area**

The last two output parameters that were analyzed were evaporation rate and coverage area. Evaporation rate was calculated using the data from the crystal monitor within the pentacene evaporator. The coverage area was calculated from the images scanned using AFM. According to the relationships seen in Figure 29 below, evaporation rate is affected only by the input current, and the coverage area does not show any strong relationships with the input factors.

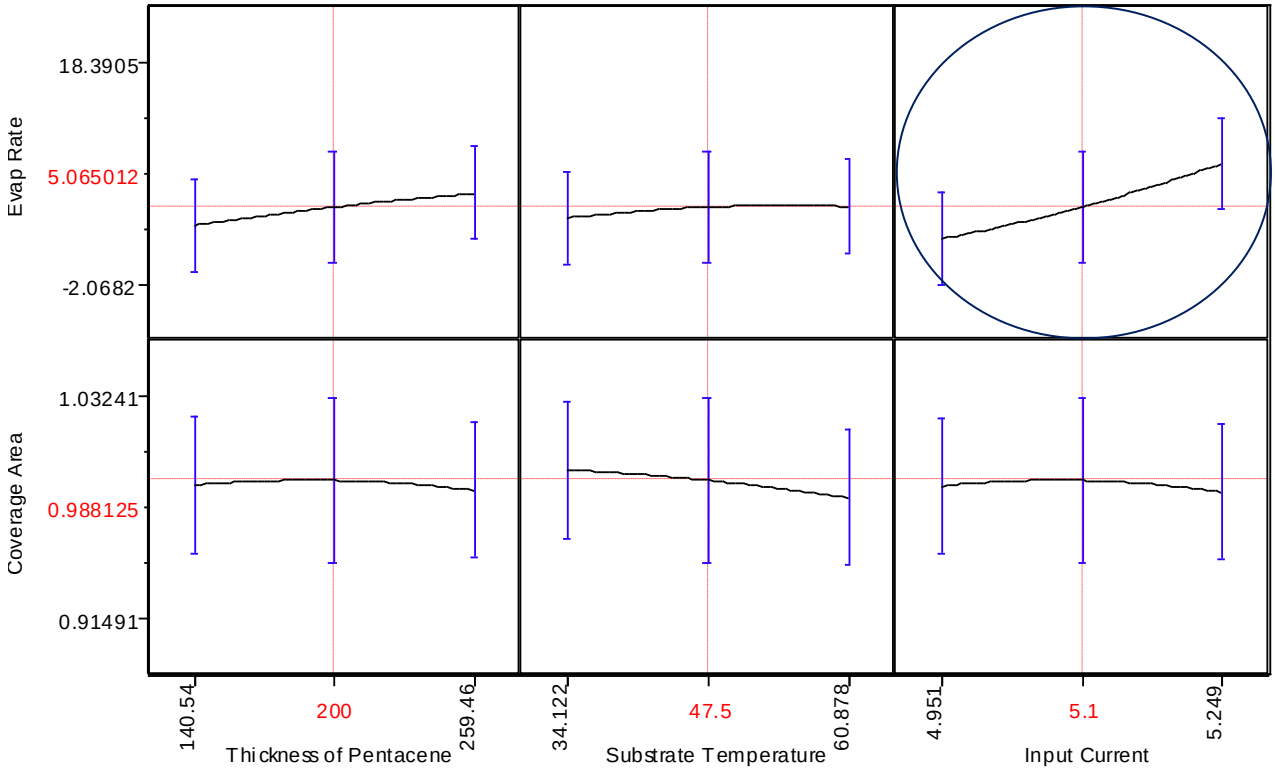


**Figure 29.** Relationship between the input parameters and evaporation rate and coverage area.

The higher the input current, the higher the temperature of the crucible holding the pentacene for evaporation. This in turn will cause a higher evaporation rate. For coverage area, none of the input factors show a statistically significant effect since the slopes are all smaller than the error bars. This is most likely due to some noise from the data extracted. One way to improve this

noise would be to use a more precise and statistically accurate tool to measure coverage area. The purpose of using a contrast tool to obtain coverage area data was to get a general idea of the trend across all of the experiments in the DOE.

Similar to the figures shown previously, Figure 30 shows the lowest and highest coverage area from samples of 2 different experiments. The evaporation rate, depending on the input current, ranged from 0.838 Å /min to 18.391 Å /min.

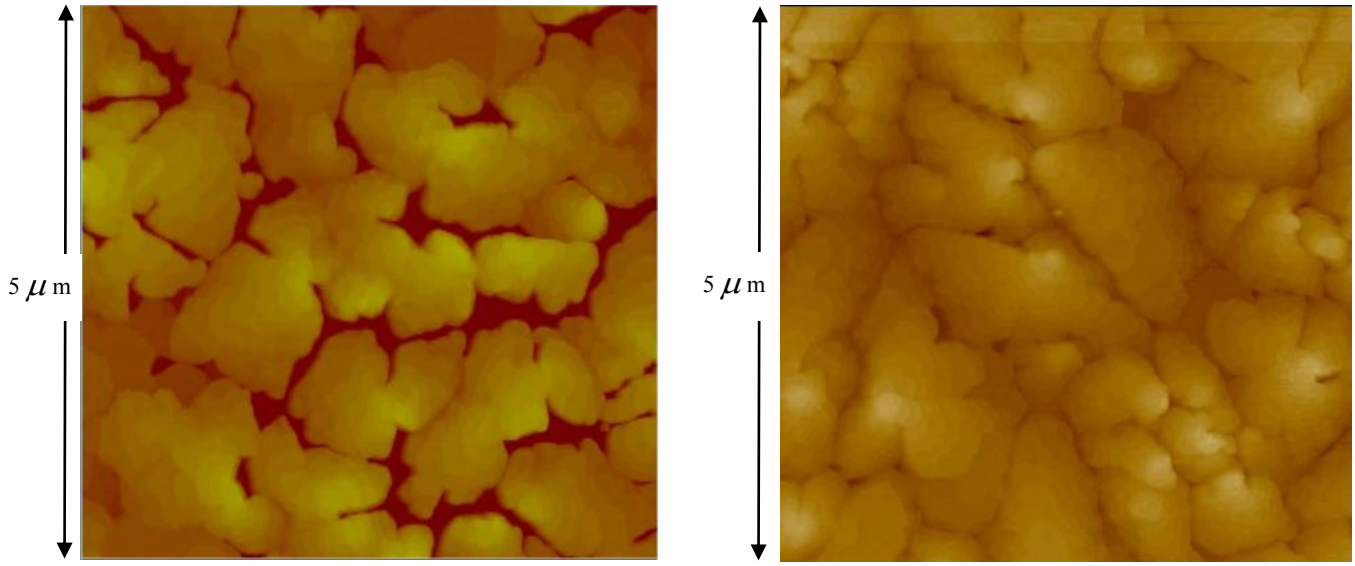


**Figure 30.** AFM Images of samples from 2 different experiments that resulted in the lowest (left) and highest (right) coverage area. The yellow area in the images represents the pentacene crystals, and the dark red area is the $SiO_2$ (dielectric) surface.

The left image with the lowest coverage area exposes a lot of the dielectric surface. The stacking of the image on the right is better, and coverage area is much higher since the dielectric surface is completely covered by the pentacene crystals.

Sections 1-5 presented thus far have highlighted the importance of the relationship of the different input parameters and their effect on the morphological and electrical characteristics of pentacene TFTs. The following section takes this a step further and integrates the DNA immobilization experiment into the data obtained so far, to arrive at the optimum conditions for highest sensitivity.

## B. Optimization of DNA Immobilization and Sensor Sensitivity

The purpose of this part of the experiment is to determine pentacene evaporation conditions that facilitate optimum DNA immobilization and highest sensitivity.

### *i. Experiment Protocol*

The experiment protocol that was followed is enlisted below. For each of the experiments in the DOE, the following steps are followed:

1) Pre-measurements of electrical characteristics of transistors on substrate (153 transistors from all of the 17 experiments) using the probe station (same set up as described on page 37)
2) Pipetting of 1.5 $\mu$L of DNA (125 Base-Pairs single strand DNA sequence synthesized by BioSynthesis, Inc) on channels of pre-measured transistors; the concentration of DNA used in this experiment was 0.5 $\mu$g/ $\mu$L
3) Immobilization of DNA on pentacene surface (in air) until buffer solution is dry
4) Washing of sample for 1-2 minutes with DI Water
5) Drying of substrate (gently)
6) Storage of transistors for a few hours in nitrogen (to neutralized any buffer solution and DI water effects)
7) Post-Measurements of electrical characteristics
8) Calculation of sensitivity of particular substrate using Ion ratio and threshold voltage shifts

The storage of the sample in nitrogen (step 6) before the post-measurement of electrical characteristics is important in order to neutralize the effects that buffer and DI water have on the pentacene surface. This was concluded based on control experiments performed using different

protocols on the similar substrates. The control experiment performed and the results obtained are discussed in the following section.

### *ii. Control Experiments*

Since pentacene is moisture sensitive, control experiments had to be performed to make sure that the effects of buffer solution and water on the pentacene transistors do not confound the DNA immobilization results. Dr. Qintao Zhang had previous shown results from control experiments he had performed using buffer solution and DI water on pentacene. The set of control experiments done this time around was to figure out what step in the process actually neutralized the effects. A few protocols were followed, and the one presented in the previous section produced the desired results. The results from the control experiments performed using this protocol is shown in Figure 31 below. $I_{dsat}$ ratio of 1 means that the electrical characteristics have not been affected.

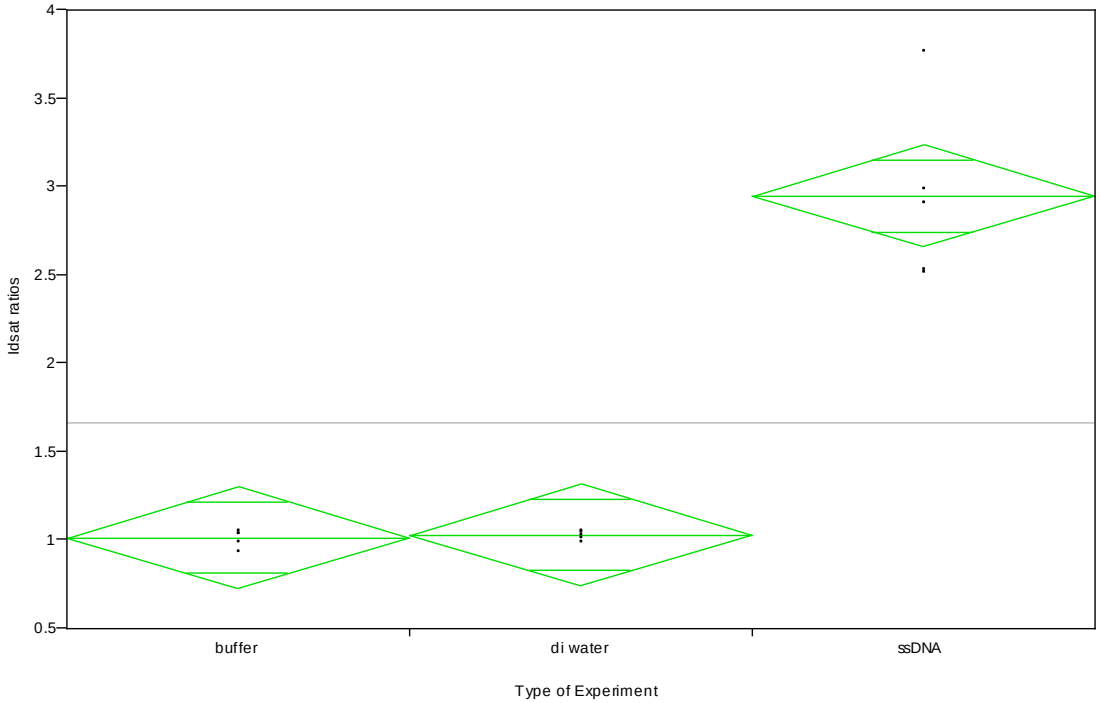


**Figure 31.** Control Experiments performed to neutralize buffer solution and DI water effects on pentacene TFTs.

The storage in nitrogen neutralized the buffer solution and DI water effects. Further experiments need to be performed to understand why the storage in nitrogen helps in this process so that the storage time and atmosphere can be optimized.

### *iii. Results: Optimization of DNA Immobilization and Sensor Sensitivity*

This section presents the results from integrating the pentacene characterization experiment with DNA. To review, the $I_{dsat}$ ratio is defined as follows:

$$\mathbf{I_{dsat}\ Ratio} = \frac{I_d\,(DrainCurre\,nt)\,AfterDNA\,\mathrm{Im}mobilizati\,on}{I_d\,BeforeDNA\,\mathrm{Im}mobilizati\,on}$$

As with previous experiments, JMP leverages the 153 points that were measured before and after DNA immobilization (for $I_{dsat}$ Ratio), to produce the graphs and relationships in Figure 32 below.

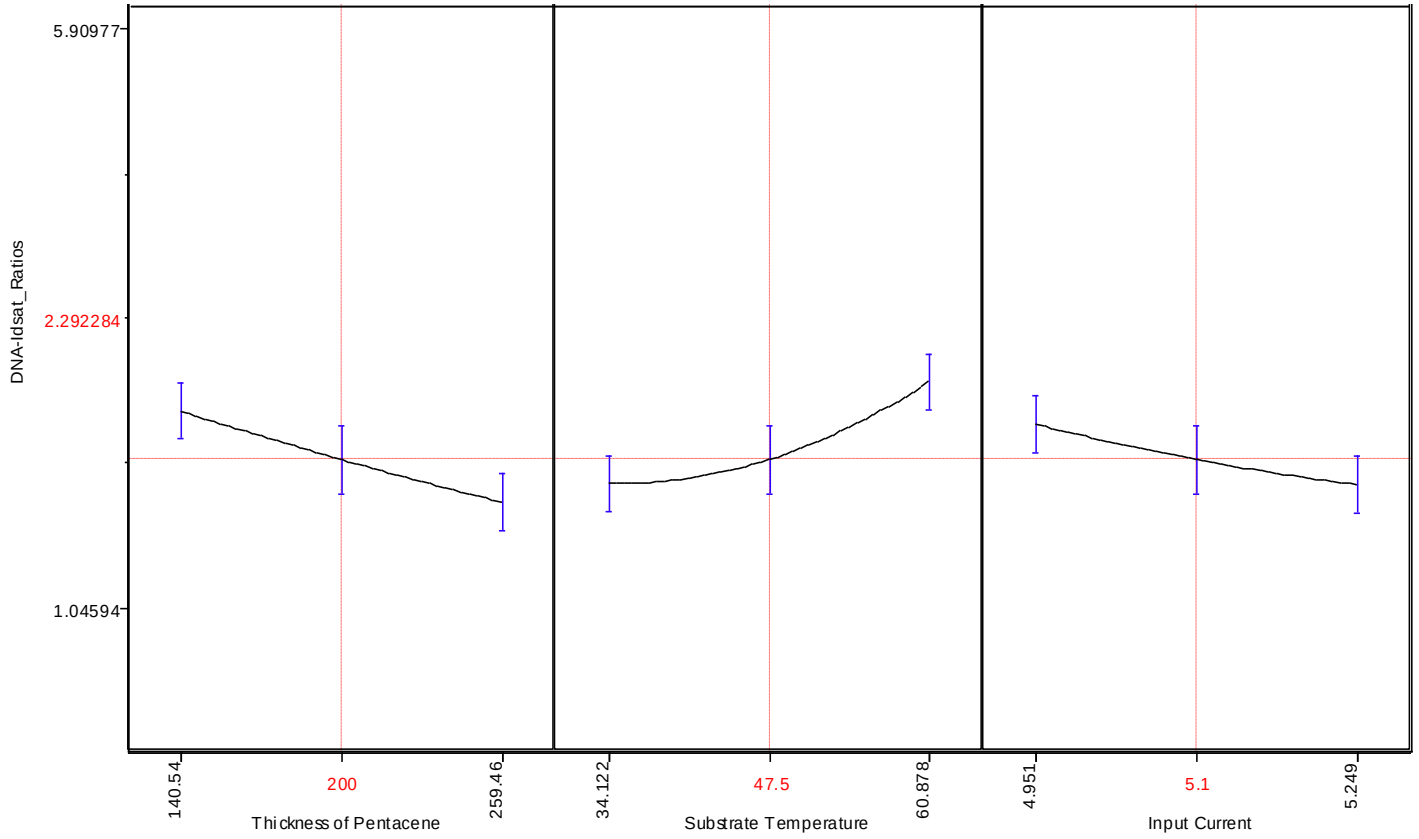


**Figure 32.** Relationship between input parameters and $I_{dsat}$ ratios.

The input parameters have already been related to the morphological and electrical characteristics. In this section, we relate the input parameters to sensor sensitivity. To begin with, as the thickness of pentacene increases, the $I_{dsat}$ ratio or sensitivity goes down. Thinner films allow the DNA to be immobilized in the channel part of the film and affect the performance more. The channel is formed in the first few monolayers (monolayer = 15 Å) of the pentacene film. Although thicker pentacene might immobilize more DNA because of higher surface roughness, the sensitivity will not be high because not all of the DNA will be immobilized in the channel part of the pentacene film to actually cause an effect.

As substrate temperature increases and input current decreases, the sensitivity increases. Higher substrate temperature and lower input current (lower deposition rate) lead to bigger grains on the surface. At thin film phases, the pentacene film growth produces a terrace like structure shown in an AFM image in Figure 33.

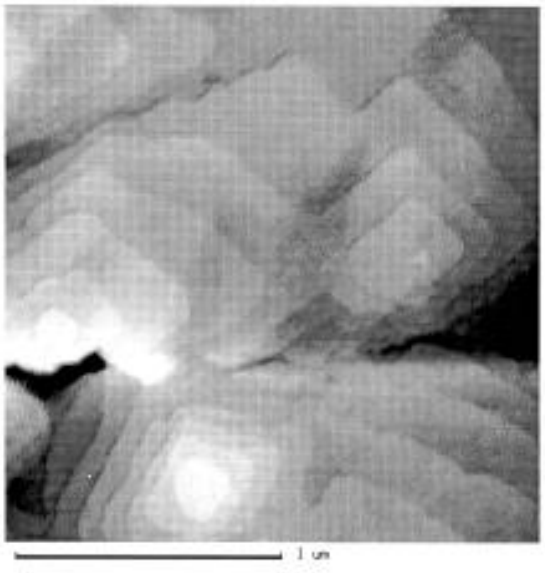

**Figure 33.** AFM Image of terrace-like formation of pentacene thin film on $SiO_2$ substrate [27].

Because of the terrace formation, the bigger the grain size, the more exposure there is to the first few monolayers of the film. In other words, bigger size allows for a wider area of exposure of

the first few monolayers of the film, where the channel forms. This is in contrast to smaller grain size, where even with the terrace formation, the channel part of the film is not widely exposed. Therefore, the bigger the grain size, the more area (in the channel part of the film) the DNA has to immobilize. This agrees very well with the data seen in Figure 32. With lower input current and higher substrate temperature, bigger grains are grown, allowing the DNA to more effectively immobilize and affect the channel part of the film, thereby causing the highest electrical shift and giving the highest sensitivity. *The sensitivity values range from 1.0456 up to 5.909.* Figure 34 takes this analysis a step further and shows how the different input parameters interact together to affect the sensitivity.

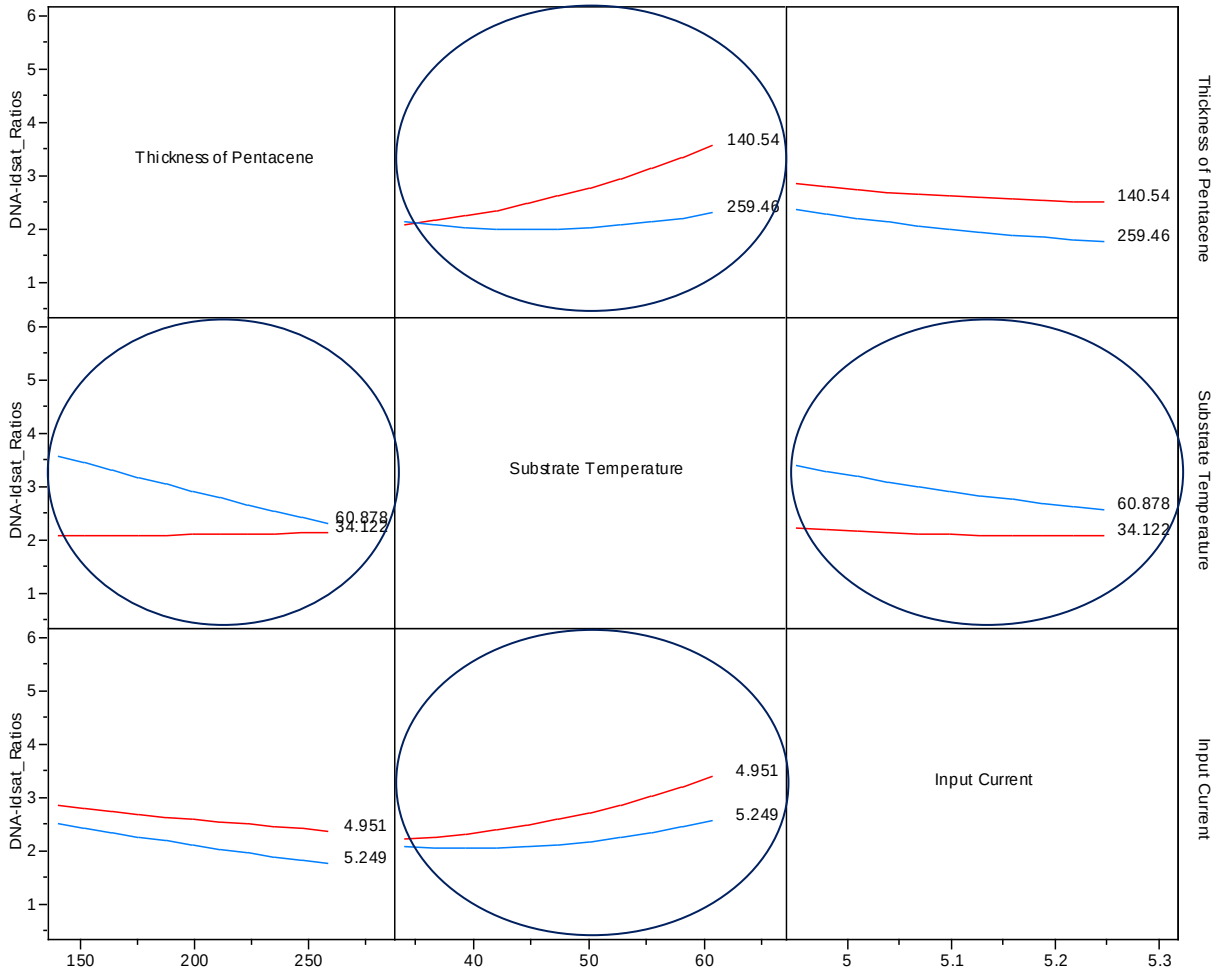


**Figure 34.** Interaction Profiler Plot for $I_{dsat}$ Ratio/Sensitivity.

We have studied impact of evaporation parameters on pentacene morphology, and tuned/ analyzed morphology to maximize the sensitivity of our OTFT platform. With thinner pentacene films, higher substrate temperature, and lower input current, we are able to achieve highest sensitivity. Results suggest that sensitivity of DNA sensor can be optimized through morphology of the film to expose as much of channel part of the film as possible for effective DNA immobilization.

# V. Conclusion and Future Work

By finding reliable methods to relate the electrical transduction behavior to physical origins, and by optimizing the pentacene film surface for highest DNA sensitivity, we have gotten closer to our goal of making a viable DNA sensor using pentacene TFTs.

Section IV.B. discussed the experimental protocol used for the DNA optimization experiment. The storage in nitrogen to neutralize effects of buffer solution and DI water was followed as a result of the performed control experiments. In order to optimize the time and atmosphere of storage in the protocol, further work needs to be done to understand the nitrogen interaction with buffer solution and DI water and its effects on the pentacene surface. Also, to make the DNA immobilization more stable and predictable, future work should focus on chemically modifying the pentacene surface to covalently bind to the DNA. This way, the orientation of the DNA is clear, and future experiments with hybridization will be more controllable. Since the goal is to be able to use this DNA detection chip for genetic disease detection, more work on hybridization detection needs to be performed. Particularly, more research needs to be performed into detecting single point mutation, known as 'single nucleotide polymorphism' with a 20-30 base pair sequence as done in medical practice today.

# VI. Sources


[1] Knowledge Systems Institute, Image of Biological Structure, *Knowledge Systems Institute.* [Online]. Available: http://distancelearning.ksi.edu/demo/bio378/DNA_files/image023.jpg . [Accessed: December 2, 2008].

[2] S. Molesa, "Ultra-Low-Cost printed electronics," Ph.D. dissertation, University of California-Berkeley, Berkeley, CA, USA, 2006.

[3] National Human Genome Research Institute, "DNA Microchip Technology," *National Human Genome Research Institute.* [Online]. Available: http://www.genome.gov/10000205. [Accessed: November 23, 2008].

[4] M. Gabig-Ciminska, "Developing nucleic acid-based electrical detection systems," *Microbial Cell Factories.,* Mar. 2006.

[5] Q. Zhang, "OTFT-Based DNA Detection System," Ph.D. dissertation, University of California-Berkeley, Berkeley, CA, USA, 2007.

[6] D. Gillespie, "A quantitative assay for DNA-RNA hybrids with DNA immobilized on a membrane," *Journal of molecular biology.,* vol. 12, pp.829, 1965.

[7] Molecular Station, Molecular Biology Images, *Molecular Station.* [Online]. Available:http://www.molecularstation.com/molecular-biology-images/data/502/557px-DNA_chemical_structure.png. [Accessed: November 23, 2008].

[8] Penn State Department of Chemistry, Image of Pentacene Structure, *Penn State Elberly College of Science.* [Online]. Available: http://www.chem.psu.edu/images/ Pentacene_JPEG.jpg. [Accessed: December 7, 2008].

[9] "Atomic force microscope," [Online]. Available: http://en.wikipedia.org/wiki/Atomic_force_ microscope. [Accessed: December 7, 2008].

[10] C. Bai, *Scanning Tunneling Microscopy and Its Application.* Springer, 1995.

[11] M. J. Heller, "DNA Microarray Technology: Devices, Systems, and Applications," *Annu. Rev. Biomed. Eng*., vol. 4,, pp.129, 2002.

[12] "Kelvin probe force microscope," [Online]. Available: http://en.wikipedia.org/wiki/Kelvin_ probe_force_microscope. [Accessed: December 5, 2008].

[13] Science Education Resource Center at Carleton College, Image of Fluorescent Microscopy System, *Science Education Resource Center at Carleton College*. [Online}. Available: http://serc.carleton.edu/images/microbelife/research_methods/microscopy/fluorescent_filters.jpg. [Accessed: December 7, 2008].

[14] "Fluorescence", [Online]. Available http://en.wikipedia.org/wiki/Fluorescence. [Accessed: November 23, 2008]

[15] Wikipedia, "What is the wavelength of blue light?" *Wiki Answers.* [Online]. Available: http://wiki.answers.com/Q/What_is_the_wavelength_of_blue_light. [Accessed: December 8, 2008].

[16] Arizona State University, "Single Molecule Spectroscopy," *Arizona State University*. [Online]. Available: http://www.public.asu.edu/~laserweb/woodbury/smf.html. [Accessed: December 11, 2008].

[17] Evans Analytical Group, "Time-of-Flight Secondary Ion Mass Spectrometry (TOF-SIMS)," *Analytical Techniques.* [Online]. Available: http://www.cea.com/techniques/analytical_ techniques/tof_sims.php. [Accessed: December 2, 2008].

[18] R. Plasun, "Optimization of VSLI Semiconductor Devices," Ph.D. dissertation, Vienna University of Technology, Vienna, Austria, 1999.

[19] JMP Statistical Discovery Software, *JMP 5.0.1a Software Manual*, 1989.

[20] S. E. Fritz Vos, "Structure and Transport in Organic Semiconductor Thin Films," Ph.D. dissertation, University of Minnesota, USA, May 2006.

[21] G. Horowitz and M .E. Hajlaoui, "Mobility in polycrystalline oligothiophene field-effect transistors dependent on grain size," *Advanced Materials,* vol.12, no.14, pp. 1046-1050, 2000.

[22] D. Knipp, D.K. Murti, B. Krusor, R. Apte, L. Jiang, J.P. Lu, B.S. Ong, and R. Street, "Photoconductivity of Pentacene Thin Film Transistors," *Materials Research Society Symposium Proceedings*, Vol. 665, pp. 207-212, 2002.

[23] A. J. Salih, S. P. Lau, J. M. Marshall, J. M. Maud, W. R. Bowen, N. Hilal, R. W. Lovitt, and P. M. Williams, "Improved thin films of pentacene via pulsed laser deposition at elevated substrate temperatures," *Appl. Phys. Letters, vol.* 69, pp. 2231, 1996.

[24] T. Minakata, H. Imai, and M. Ozaki, "Electrical properties of highly ordered and amorphous thin films of pentacene doped with iodine," *Journal of Applied Physics, vol.* **72**, pp. 4178, 1992.

[25] J.W. Chang, H. Kim, J.K. Kim, B. K. Ju, J. Jang, and Y.H. Lee, "Structure and Morphology of Vacuum-Evaporated Pentacene as a Function of the Substrate Temperature," *Journal of the Korean Physical Society,* Vol. 42, pp. S647-S651, February 2003.

[26] Wikipedia, "Ostwald ripening," *Wikipedia,* [Online]. Available: http://en.wikipedia.org/wiki /Ostwald_ripening. [Accessed: December 8, 2008].

[27] I. P. M. Bouchoms, W. A. Schoonveld, J. Vrijmoeth, and T. M. Klapwijk**,** "Morphology identification of the thin film phases of vacuum evaporated pentacene on $SiO_2$ substrates," *Synthetic Metals*, Vol. 104, Issue 3, pp.175-178, July 1999.

[28] K. Puntambekar, "Characterization of Structural and Electrostatic Complexity in Pentacene Thin Films By Scanning Probe Microscopy," Ph.D. dissertation, University of Minnesota, USA, October 2005.

[29] K.O Lee and T.T. Gan, "Space-Charge-Limited Currents in Evaporated Films of Pentacene," *Physics Stat. Solutions, vol. 43, p. 565, 1977.*

# APPENDIX

## MASS SPECTRA RESULTS FROM TOF-SIMS Analysis

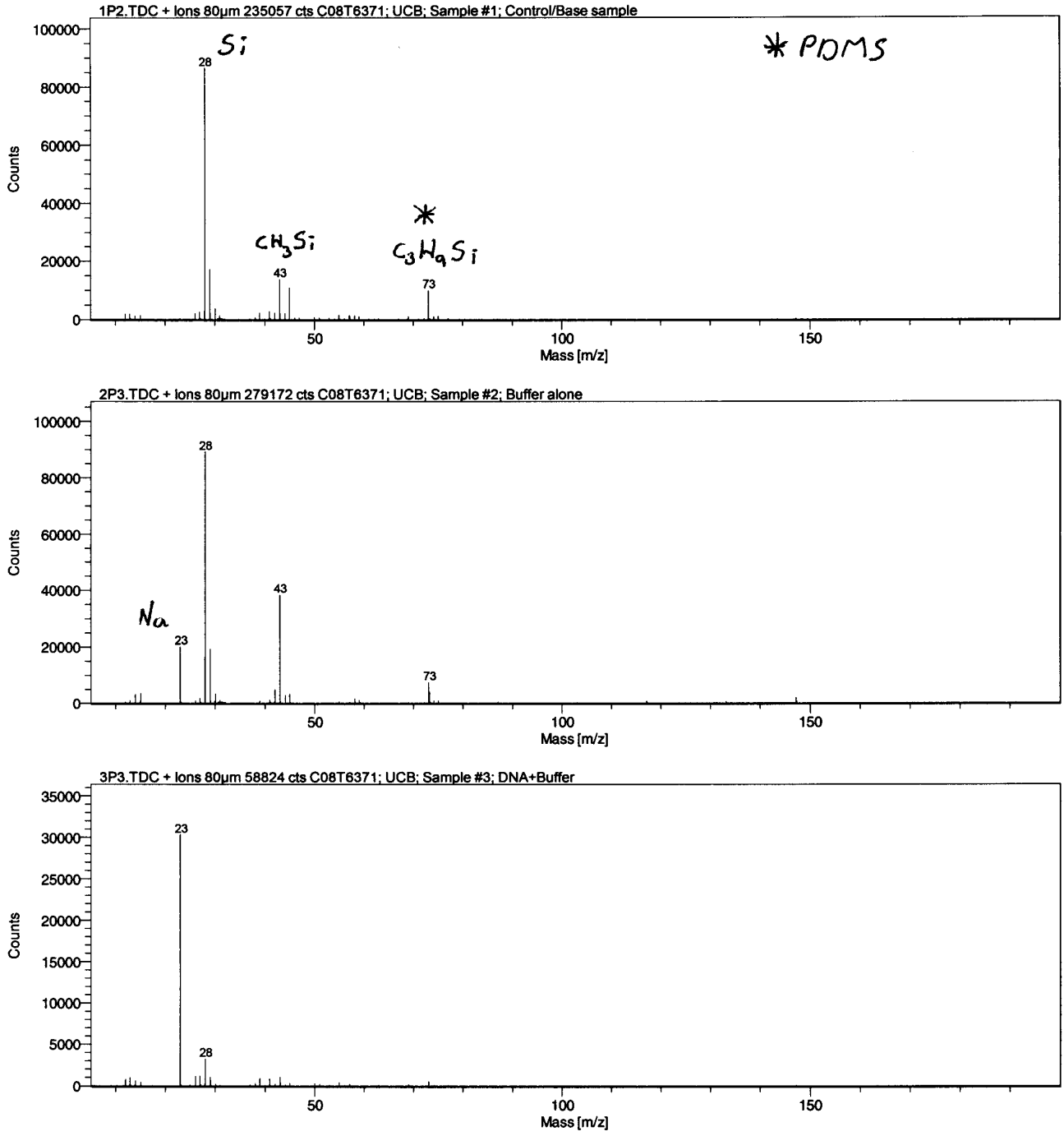


**Figure 35.** Mass Spectra of positive ions of interest for samples 1 to 3; Mass to Charge Ratio: 0-200

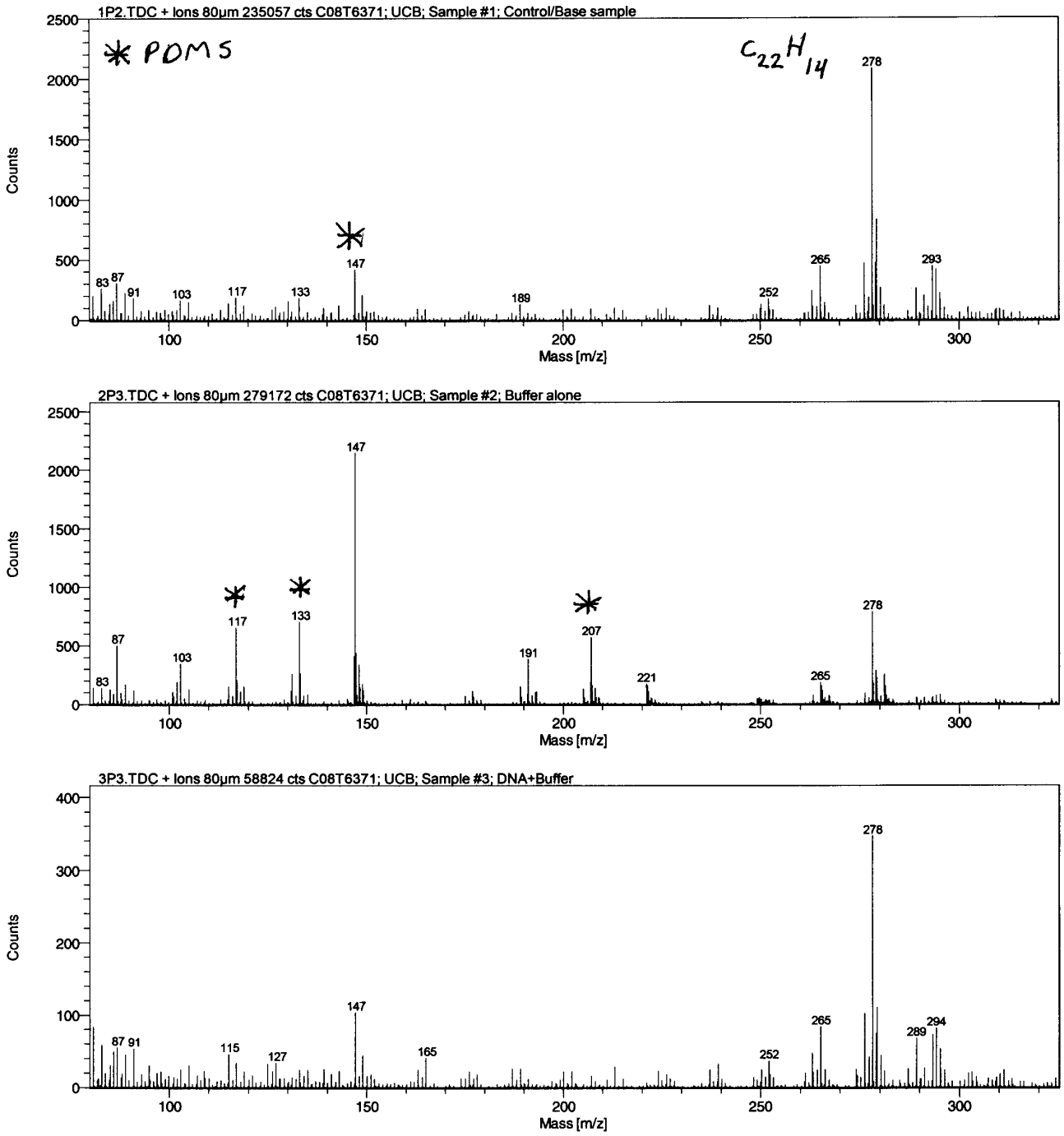


**Figure 36.** Mass Spectra of positive ions of interest for samples 1 to 3; Mass to Charge Ratio: 100-300

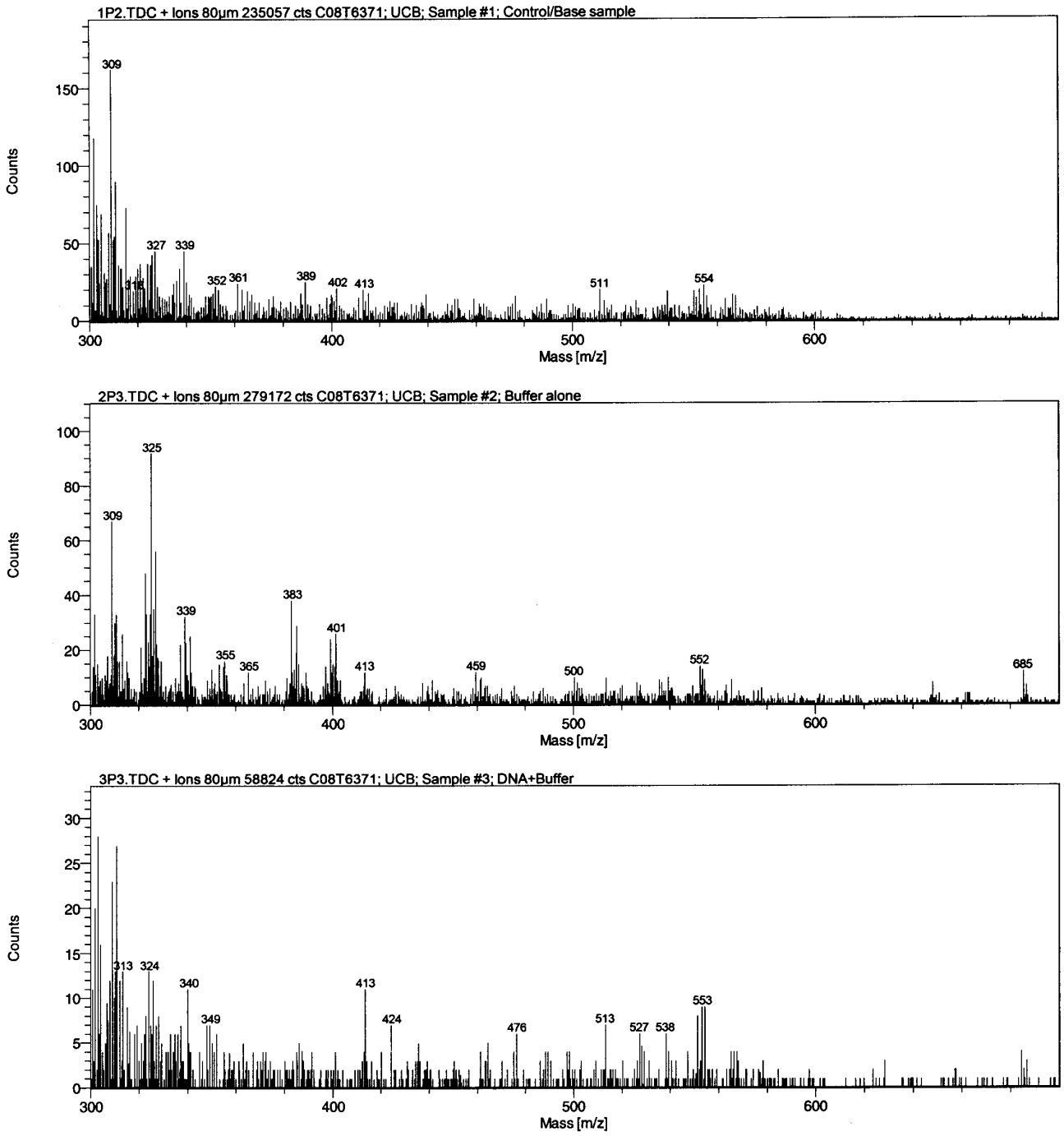


**Figure 37.** Mass Spectra of positive ions of interest for samples 1 to 3; Mass to Charge Ratio: 300-700

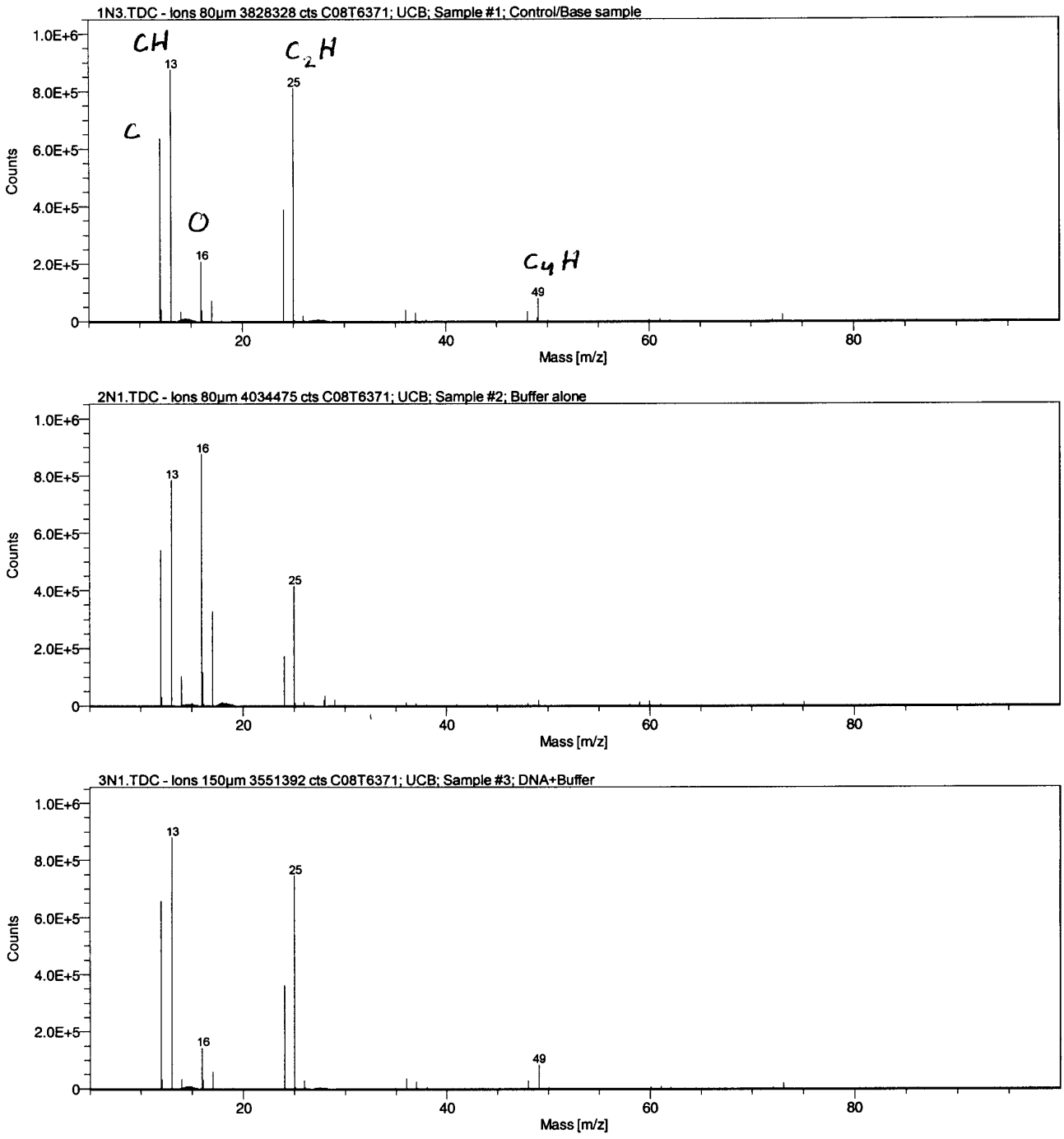


**Figure 38.** Mass Spectra of negative ions of interest for samples 1 to 3; Mass to Charge Ratio: 0-100

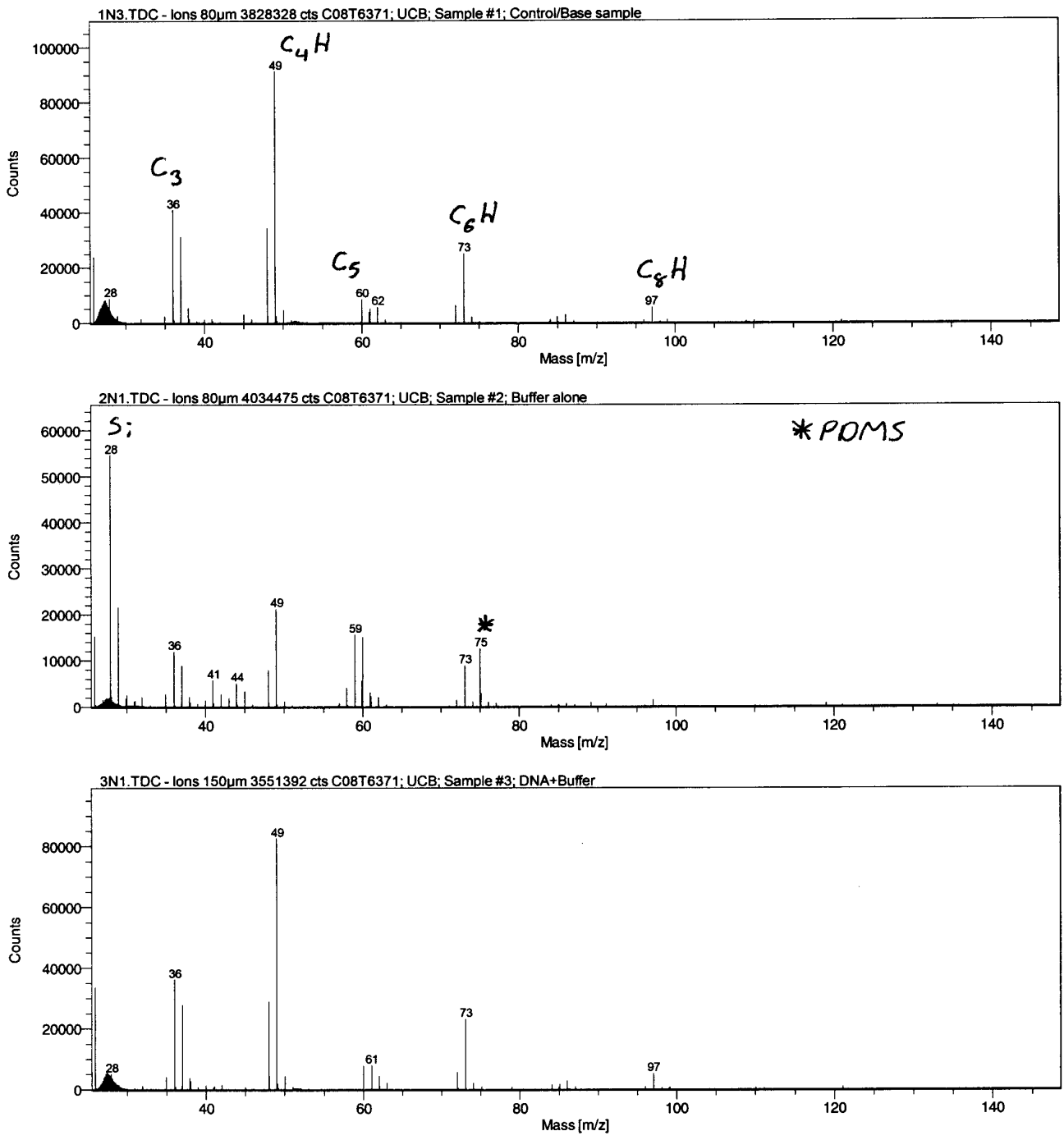


**Figure 39.** Mass Spectra of negative ions of interest for samples 1 to 3; Mass to Charge Ratio: 0-140

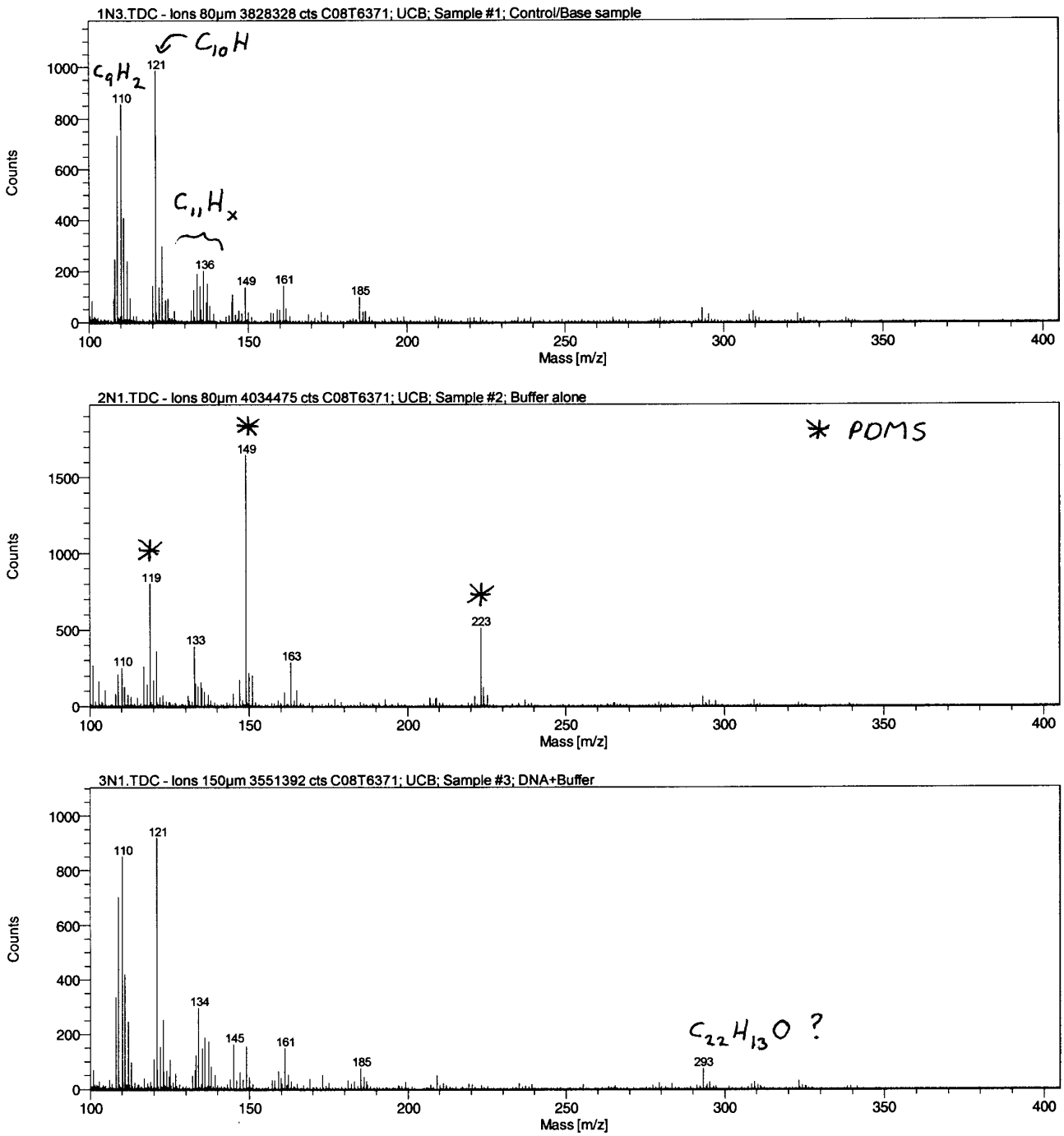


**Figure 40.** Mass Spectra of negative ions of interest for samples 1 to 3; Mass to Charge Ratio: 100-400